Techno-computing Journal 2(1) 1-28(2026)
https://doi.org/10.71170/tecoj.2026.2.1.1-28

Research Paper

A Novel Hybrid Intelligence Framework for Predicting Strength in Sustainable Concrete Incorporating Animal Bone Ash

Daha S. Aliyu[1,5*], Hafizu Hamza Ali[2], Haruna Ibrahim[3], Mahmoud M. Farouq[4,5]
[1]*School of Engineering, Newcastle University Upon Tyne, NE1 7RU, United Kingdom*
[2]*School of Technology, Kano State Polytechnic, Nigeria*
[3]*Department of Civil Engineering, Federal University Wukari, Taraba State*
[4]*School of Architecture, University of Nottingham, United Kingdom*
[5]*Department of Civil Engineering, Aliko Dangote University of Science and Technology, Wudil*
**Corresponding Author Email: engrshanono@kustwudil.edu.ng*

Abstract

The accurate prediction of compressive strength in sustainable concrete composites remains a formidable challenge owing to the inherently complex, non-linear, and multi-parametric nature of hydration reactions and pozzolanic interactions. This study presents a novel hybrid intelligence framework for multi-mixture modeling of compressive strength in lightweight concrete incorporating animal bone ash (ABA) as a partial cement replacement. A comprehensive experimental dataset comprising 45 lightweight concrete cube specimens (5 ABA replacement levels × 3 curing ages × 3 replicates) was developed, with cement partially replaced at 0%, 5%, 10%, 15%, and 20% and coarse aggregate fully replaced with pumice. Compressive strength measurements were obtained at 7, 14, and 28 days of curing. Five distinct data-driven algorithms were employed: Multilayer Perceptron (MLP), Least Square Support Vector Machine (LSSVM), Adaptive Neuro-Fuzzy Inference System (ANFIS), Hammerstein-Wiener (HW), and Autoregressive Integrated Moving Average (ARIMA). Subsequently, hybrid ARIMA-MLP, ARIMA-LSSVM, ARIMA-ANFIS, and ARIMA-HW models were developed to capture both trend and non-linear patterns inherent in the strength development process. Model performance was evaluated using the determination coefficient (R^2), root mean square error (RMSE), mean absolute error (MAE), and performance index (PI), complemented by Taylor diagram visualization. Quantitative analysis revealed that the HW model demonstrated superior predictive capability for 5% replacement mixtures, achieving R^2 values of 0.94, 0.92, and 0.91 at 7, 14, and 28 days, respectively. The ANFIS model exhibited optimal performance for 15% replacement scenarios, with R^2 values of 0.93, 0.91, and 0.90 across the curing periods. Hybrid ARIMA-ANFIS and ARIMA-HW models substantially outperformed their standalone counterparts, with ARIMA-ANFIS achieving the highest overall predictive accuracy (R^2 = 0.98, RMSE = 0.02 N/mm², MAE = 0.01 N/mm²) for the 15% replacement mixture at 28 days. The proposed hybrid intelligence framework demonstrates significant potential as a reliable decision-support tool for optimizing sustainable concrete mixtures incorporating agro-industrial waste materials.

Keywords: Animal Bone Ash, Lightweight Concrete, Compressive Strength, Hybrid Intelligence, Multi-Mixture Modeling

1. Introduction

Concrete remains the most extensively utilized construction material globally, with annual production exceeding 10 billion metric tons, making it the second most consumed substance after water [1], [2]. The environmental implications of this massive production are profound, particularly concerning ordinary Portland cement (OPC), which contributes approximately 8% of global anthropogenic carbon

(Received 25 Jan 2026; revised 10 March 2026; accepted 11 March 2026; first published online 19 March 2026);

dioxide emissions [3], [4]. This environmental burden, coupled with the escalating demand for sustainable construction practices, has catalyzed extensive research into alternative cementitious materials derived from agricultural and industrial waste streams [5], [6]. Simultaneously, the construction industry has witnessed growing interest in lightweight concrete (LWC) technologies, which offer substantial advantages over conventional normal-weight concrete in multi-story building applications. According to established standards [7], lightweight concrete is defined as having an oven-dry density typically ranging from 300 to 1850 kg/m³, compared to 2200–2600 kg/m³ for conventional normal-weight concrete. This reduced density translates to significant reductions in structural dead loads, foundation dimensions, and seismic forces. Furthermore, LWC exhibits enhanced thermal insulation properties, improved fire resistance, and superior durability characteristics under appropriate mixture designs [8].

ABA represents an underexplored, yet promising supplementary cementitious material (SCM) derived from the substantial quantities of bone waste generated by the meat processing industry. Globally, the livestock sector produces approximately 130 million tons of bone waste annually, presenting both environmental disposal challenges and opportunities for value-added utilization [9], [10]. The chemical composition of calcined bone predominantly comprises calcium phosphate [$Ca_3(PO_4)_2$] in the form of hydroxyapatite, along with calcium oxide and minor quantities of other minerals [11]. This composition suggests potential pozzolanic or hydraulic behavior when incorporated into cementitious systems. The experimental investigation of concrete properties, particularly compressive strength development, remains the cornerstone of mixture proportioning and quality assurance [12], [13]. However, conventional experimental approaches are inherently time-consuming, resource-intensive, and limited in their capacity to explore the multidimensional parameter space characterizing modern concrete composites [14], [15]. The hydration process in cementitious systems involves complex thermo-hydro-chemo-mechanical interactions characterized by strong non-linearity and time-dependent behavior. [16], [17],[18]. In recent decades, data-driven modeling approaches have emerged as powerful complementary tools for investigating and predicting the behavior of construction materials [19], [20], [21]. Artificial intelligence (AI) and machine learning (ML) algorithms offer the capability to capture intricate non-linear relationships within experimental datasets without requiring explicit formulation of underlying physical mechanisms [22], [23], [24]. These methodologies have been successfully applied to diverse problems in concrete technology, including compressive strength prediction [14], [25], mix proportion optimization [15], durability assessment [26], and rheological property estimation [27].

Artificial neural networks (ANNs), particularly MLP architectures, have been extensively employed for concrete property prediction owing to their universal approximation capabilities and relative simplicity of implementation [28], [29]. Several studies have demonstrated the efficacy of ANN-based approaches for modeling compressive strength of conventional and modified concrete mixtures [30], [31]. However, ANNs are susceptible to overfitting, local minima entrapment, and sensitivity to network architecture and training parameters [32], [33]. Support vector machines (SVM) and their least squares variant (LSSVM) represent an alternative paradigm in statistical learning theory, offering enhanced generalization capability through structural risk minimization [34], [35]. LSSVM has demonstrated promising performance in various civil engineering applications, including concrete strength modeling [36], [37]. The LSSVM formulation reduces computational complexity by solving a system of linear equations rather than the quadratic programming problem characteristic of standard SVM [35].

However, ANFIS synergistically integrate the learning capabilities of neural networks with the interpretability of fuzzy logic systems [38], [39]. This hybrid paradigm is particularly well-suited for modeling systems characterized by uncertainty, imprecision, and complex non-linear interactions, features prominently exhibited by cementitious materials [40], [41]. ANFIS has been successfully applied to predict properties of various concrete types, including high-performance concrete [42], self-compacting concrete [41], and recycled aggregate concrete [43]. The HW model, a block-oriented nonlinear system identification approach, has gained increasing attention in engineering applications [44], [45]. This structure decomposes the system dynamics into cascaded linear and nonlinear blocks, offering parsimonious representation of complex nonlinear behavior [46]. Despite its demonstrated effectiveness in chemical process control [47], bioprocess engineering [48], and hydrological modeling [33], the HW framework remains largely unexplored in construction materials research. ARIMA models, originating from time series analysis [49], have been employed to capture temporal dependencies in strength development processes [50]. However, the inherent linearity assumption of ARIMA models limits their applicability to strongly nonlinear phenomena characteristic of cement hydration [51], [52].

Recognizing that no single modeling paradigm universally outperforms others across all datasets and problem contexts a principle encapsulated in the "no free lunch" theorem [53] recent research has increasingly focused on hybrid modeling approaches. Hybrid models synergistically combine the strengths of multiple paradigms while mitigating their individual limitations [52], [54]. The fundamental premise underlying hybrid time series modeling is that real-world processes often exhibit both linear and nonlinear components, which may be optimally captured by different modeling methodologies [52], [55]. In the context of concrete strength modeling, several hybrid approaches have been investigated. Nourani et al. (2012) [56] employed wavelet-ANN hybrids for modeling compressive strength of concrete containing mineral admixtures. Gupta et al. (2019) [33] developed hybrid ANFIS-particle swarm optimization models for predicting strength properties of high-performance concrete. Similarly, Chou and Pham (2013) [57] compared hybrid artificial intelligence models for estimating compressive strength of high-performance concrete, demonstrating the superior performance of ensemble and hybrid approaches over standalone algorithms. Despite these advances, several research gaps persist. First, the application of hybrid intelligence frameworks for modeling lightweight concrete incorporating ABA remains unexplored. Second, the comparative performance of emerging nonlinear system identification approaches (e.g., HW) relative to established AI paradigms has not been systematically evaluated for this application domain. Third, the potential of hybrid ARIMA-AI architectures for capturing both temporal (curing age) and compositional (replacement level) dependencies in strength development has not been investigated.

Despite these advances, several critical research gaps persist. First, current predictive models for sustainable concrete incorporating ABA are largely mixture-specific, developing separate algorithms for each replacement level. This approach fails to capture the continuous, interactive effects between cement replacement and curing age, limiting their utility for interpolating to untested mixture proportions. Second, while standalone AI models (ANN, ANFIS, SVM) have been applied to concrete strength prediction, they struggle to simultaneously capture the linear trend component of strength development over time and the complex non-linear interactions introduced by pozzolanic materials. Specifically, these models cannot adequately decompose the strength development process into its constituent linear and non-linear components, often overfitting to training data or failing to generalize across multiple mixture proportions. Third, emerging non-linear system identification approaches such as the HW framework which separately models input non-linearity, linear dynamics, and output non-linearity remain unexplored in construction materials research despite their theoretical alignment with concrete hydration processes. The necessity of hybrid ARIMA-AI modelling arises from the fundamental nature of compressive strength development in cementitious systems. The process inherently comprises both linear and non-linear components: a predictable linear trend associated with progressive cement hydration under standard curing conditions, and complex non-linear fluctuations arising from pozzolanic interactions, microstructural evolution, and threshold effects at specific replacement levels. Conventional ARIMA models, while effective at capturing the linear trend, cannot accommodate the non-linear dynamics introduced by ABA incorporation. Conversely, standalone AI models, though capable of learning non-linear relationships, treat the entire strength development process as a black box, failing to explicitly model the underlying temporal structure. Hybrid ARIMA-AI modelling addresses these limitations by sequentially decomposing the problem: ARIMA first captures the linear trend component, producing residuals that contain purely non-linear information, which is then modelled by AI algorithms. This synergistic approach ensures that both the predictable time-dependent behaviour and the complex compositional interactions are accurately represented, offering superior predictive accuracy and generalizability across multiple mixture proportions.

The present study addresses these gaps through the following specific objectives: (i) To experimentally characterize the compressive strength development of lightweight concrete incorporating 0–20% ABA as partial cement replacement at 7, 14, and 28 days of curing, (ii)To develop and compare five standalone intelligence models (MLP, LSSVM, ANFIS, HW, and ARIMA) for predicting compressive strength across multiple mixture proportions and curing ages, (iii)To propose and evaluate hybrid ARIMA-MLP, ARIMA-LSSVM, ARIMA-ANFIS, and ARIMA-HW models that capture both linear and nonlinear components of the strength development process and (iv)To assess model performance using comprehensive statistical indicators and visualization techniques, including Taylor diagrams. In this study, multi-mixture modeling refers to the development of predictive models that simultaneously capture compressive strength behavior across multiple replacement levels (0%, 5%, 10%, 15%, and 20%) and curing ages (7, 14, and 28 days). Unlike mixture-specific modeling which develops separate models for each replacement level, this unified approach enables interpolation to untested compositions and provides a holistic representation of the combined effects of mixture proportion and curing age on

strength development. The novelty of this work is manifested in multiple dimensions. First, this study represents the first application of HW modeling to predict compressive strength of sustainable concrete composites. Second, the hybrid ARIMA-HW framework is introduced for the first time in construction materials research. Third, this investigation provides the most comprehensive comparative evaluation of standalone and hybrid intelligence algorithms for modeling ABA-modified lightweight concrete. Fourth, the multi-mixture modeling approach, simultaneously considering varying replacement levels and curing ages, offers enhanced practical utility compared to mixture-specific models. Fifth, this study contributes to the broader literature on sustainable construction by demonstrating the feasibility of predicting the performance of waste-derived cementitious materials using advanced computational techniques.

2. Materials and Methods

2.1 Materials Characterization

2.1.1 Cement

Ordinary Portland cement (OPC) conforming to BS EN 197-4:2004 [58] requirements was employed throughout this investigation. The cement, commercially available as "Dangote Portland Cement" (Type I, general-purpose), was obtained from the Wudil market, Kano State, Nigeria, This goes with relevant standards.

2.1.2 Fine Aggregate

Natural river sand sourced from the Wudil River was utilized as fine aggregate. The sand was air-dried and subjected to sieve analysis in accordance with BS EN 12620:2002 [59]. The physical properties of the fine aggregate are summarized in Table 1, with the particle size distribution illustrated in Fig. 1. The fineness modulus of 5.4 indicates the presence of a notable coarse fraction within the sand, which may influence workability and water demand. The specific gravity of 2.65 falls within the typical range for natural sands [12].

***Table 1**: Physical properties of fine aggregate*

Property	Moisture content (%)	Bulk density (compacted), kg/m³	Bulk density (uncompacted), kg/m³	Specific gravity	Fineness modulus	Void ratio
Value	1.12	1555	1422	2.65	5.4	0.46

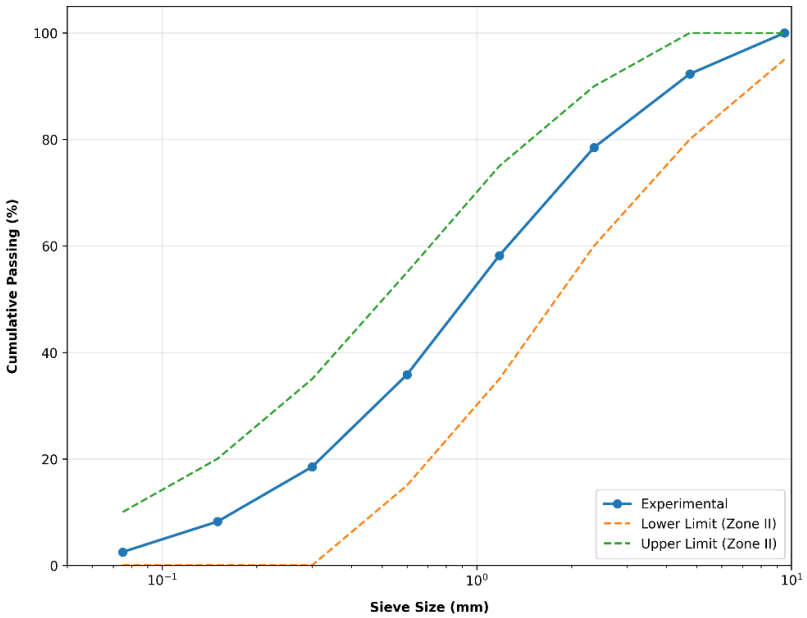

***Figure 1**: Particle size distribution of fine aggregate*

2.1.3 Coarse Aggregate (Normal Weight)

Crushed granite aggregate with nominal maximum size of 20 mm (passing 20 mm and retained on 10 mm sieve) was obtained from a local quarry site for control mixture preparation. The physical properties of the normal-weight coarse aggregate are presented in Table 2, with water absorption characteristics detailed in Table 3.

***Table 2**: Physical properties of normal-weight coarse aggregate*

Property	**Moisture content (%)**	**Bulk density (compacted), kg/m³**	**Bulk density (uncompacted), kg/m³**	**Specific gravity**	**Void ratio**
Value	0.6	1668	1503	2.60	0.42

***Table 3**: Water absorption characteristics of 20 mm gravel*

Trial Number	**1**	**2**	**3**
Weight of can (g)	22.7	27.9	19.9
Weight of can + wet sample (g)	91.8	65.8	63.9
Weight of can + dry sample (g)	91.3	65.5	63.6
Weight of dry sample (g)	68.6	37.6	44.0
Increase in mass (g)	0.5	0.3	0.3
Absorption (%)	0.73	0.80	0.68
Average absorption (%)	**0.74**		

2.1.4 Pumice (Lightweight Aggregate)

Pumice, a volcanic rock with vesicular texture formed during rapid cooling of solidified magma, was employed as lightweight coarse aggregate. The pumice was obtained from Kurmi market, Kano, and crushed to achieve 20 mm maximum aggregate size (passing 20 mm, retained on 10 mm). The material exhibits low crystalline structure, with silica (SiO_2) and alumina (Al_2O_3) constituting the primary chemical components. The physical properties of pumice are presented in Table 4.

***Table 4**: Physical properties of pumice lightweight aggregate*

Property	**Value**
Bulk density (kg/m³)	1500
Specific gravity	1.95
Water absorption (%)	18.5
Nominal maximum size (mm)	20
Particle shape	Angular, vesicular
Color	Light gray to white
Surface texture	Rough, porous

2.1.5 Animal Bone Ash

ABA was produced from cattle bones obtained from the Kano abattoir. The production process involved several stages:

1. Cleaning and preparation: Bones were thoroughly washed to remove adhering tissue and organic matter, followed by natural drying to reduce moisture content.

2. Oven drying: Bones were oven-dried at 105 ± 5°C for 24 hours to achieve constant weight, ensuring minimal moisture content prior to combustion.

3. Calcination: Dried bones were subjected to controlled combustion in a metal clinker using kerosene as fuel. The calcination temperature was estimated to reach approximately 600–800°C based on the characteristics of kerosene combustion in a controlled environment. The controlled environment minimized contamination and ash loss while ensuring complete combustion.

4. Cooling and grinding: The resulting ash were allowed to cool gradually, then pulverized to fine powder using a mechanical grinder.

5. Sieving: The ground ash was sieved through 75 μm sieve to ensure uniformity and remove oversized particles.

The chemical composition of ABA is fundamentally characterized by calcium phosphate minerals deposited within a soft organic matrix. According to Vaughan (1975), bone tissue comprises approximately 65–70% inorganic minerals (primarily hydroxyapatite, $Ca_{10}(PO_4)_6(OH)_2$), with the remainder being organic collagen and water. Upon calcination, the organic phase is eliminated, leaving a residue rich in calcium phosphate and calcium oxide. Table 5 presents the typical oxide composition of ABA.

***Table 5**: Typical oxide composition of ABA*

Oxide	CaO	P_2O_5	SiO_2	Al_2O_3	Fe_2O_3	MgO	SO_3	K_2O	Loss on ignition
Composition (%)	45-55	35-42	2-5	1-3	0.5-2	0.5-2	0.1-0.5	0.1-0.3	2-5

2.1.6 Water

Potable water sourced from a borehole within Wudil town was utilized for all mixing and curing operations. The water conformed to the requirements of BS 3148 (1980) [60] for concrete mixing water.

2.2 Mixture Proportions and Experimental Design

The experimental program was designed to investigate the compressive strength of lightweight concrete incorporating varying levels of ABA as partial cement replacement. A control mixture (conventional concrete with normal-weight aggregate and 0% ABA) was prepared for baseline comparison. Lightweight concrete mixtures were produced by fully replacing coarse aggregate with pumice, while cement was partially replaced with ABA at five levels: 0%, 5%, 10%, 15%, and 20%. All mixtures were designed for target strength corresponding to M20 grade concrete (characteristic strength of 20 N/mm² at 28 days) using the BS Standard method of mix design. The water-cement ratio was maintained constant at 0.5 across all mixtures to isolate the effect of ABA replacement. Table 6 summarizes the mixture proportions for the various concrete types investigated.

***Table 6**: Mixture proportions for concrete mixtures (per m³)*

Mixture ID	**Cement (kg)**	**ABA (kg)**	**Fine Aggregate (kg)**	**Coarse Aggregate (kg)**	**Pumice (kg)**	**Water (kg)**	**w/c Ratio**
Control (Conventional)							
M20-Control	380	0	650	1200	0	190	0.50
Lightweight Mixtures							
LWC-0%	380	0	650	0	860	190	0.50
LWC-5%	361	19	650	0	860	190	0.50
LWC-10%	342	38	650	0	860	190	0.50
LWC-15%	323	57	650	0	860	190	0.50
LWC-20%	304	76	650	0	860	190	0.50

2.3 Preparation and Curing

For each mixture proportion, nine 150 mm × 150 mm × 150 mm cube specimens were cast, providing three replicates for each testing age (7, 14, and 28 days). A total of 54 specimens were prepared: 9 control conventional concrete cubes and 45 lightweight concrete cubes (9 specimens × 5 replacement levels). The mixing procedure followed standard practice: dry materials were homogenised before water was added, then mechanical mixing continued until a uniform consistency was achieved. Workability was assessed using the slump test (BS 1881: Part 102, 1983) and the compaction factor test (BS 1881: Part 103, 1983). Fresh concrete was placed in moulds in three layers, each layer compacted using a vibrating table to ensure adequate consolidation. Specimens were demolded after 24 ± 2 hours and transferred to curing tanks maintained at 20 ± 2°C until the designated testing age.

2.4 Testing Procedures

Compressive strength testing was conducted in accordance with BS EN 12390-3:2001 [61] using a compression testing machine with 2000 kN capacity. Load was applied continuously at a rate of 2.5 kN/s until specimen failure. The maximum load at failure was recorded, and compressive strength was calculated as:

$$f_c = P/A \quad (1)$$

where f_c is compressive strength (N/mm²), P is failure load (N), and A is cross-sectional area (mm²).

2.5 Experimental Results

The experimental results for density and compressive strength at 7, 14, and 28 days are presented in Figure 2, with mixture designations as follows: The experimental observations indicate that lightweight concrete density ranged from 2391 to 2658 kg/m³, with most specimens falling below 2600 kg/m³, confirming the lightweight characteristics achieved through pumice incorporation. The control conventional concrete (not shown in the Table) exhibited a density of approximately 2400 kg/m³ with a 28-day compressive strength of 25.4 N/mm².

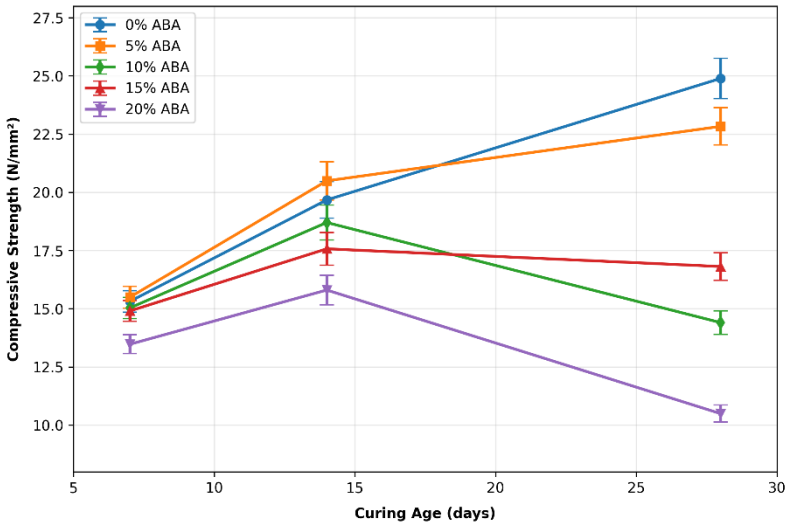

***Figure 2**: Compressive strength development of lightweight concrete mixtures at different curing ages*

The standard deviations for compressive strength measurements ranged from 0.32 to 1.87 N/mm² across all mixtures and curing ages, with coefficients of variation averaging 6.8% (range: 2.1% to 12.4%). The highest variability was observed for the 20% ABA mixture at 28 days (SD = 1.87 N/mm², CV = 17.8%), while the lowest variability occurred for the 5% mixture at 7 days (SD = 0.32 N/mm², CV = 2.1%). These values indicate acceptable experimental precision and support the reliability of mean

values used for model development. Workability characteristics, assessed through slump and compaction factor tests, are summarized in Tables 7 and 8.

***Table 7**: Slump test results for lightweight concrete mixtures*

S/N	Replacement Level	Slump Height (mm)	Slump Type
1	0% (A)	16	Shear
2	5% (B)	18	Shear
3	10% (C)	18	Shear
4	15% (D)	23	Shear
5	20% (E)	30	Shear

***Table 8**: Compaction factor test results*

Sample	Un-Compacted Weight (kg)	Compacted Weight (kg)	Compaction Factor
A (0%)	12.98	14.30	0.91
B (5%)	14.23	15.28	0.93
C (10%)	14.02	15.19	0.92
D (15%)	13.14	14.90	0.88
E (20%)	13.21	14.88	0.89

The increasing slump values with higher ABA replacement levels suggest improved workability, possibly attributable to the filler effect and morphological characteristics of bone ash particles. Compaction factor values ranging from 0.88 to 0.93 indicate adequate workability for all mixtures (Neville, 2011).

3.0 Methodology (Data-Driven Modeling Framework)

3.1 Overview of Modeling Approach

The Modeling framework employed in this study comprises two principal phases: (1) development and evaluation of five standalone intelligence models (MLP, LSSVM, ANFIS, HW, and ARIMA) for predicting compressive strength across multiple mixture proportions and curing ages; and (2) formulation of hybrid ARIMA-AI models (ARIMA-MLP, ARIMA-LSSVM, ARIMA-ANFIS, and ARIMA-HW) to capture both linear and nonlinear components of the strength development process. The underlying premise for hybrid modeling follows the formulation proposed by Zhang in 2003. The schmatic diagram of the flowchart is shown in Fig. 3.

3.2 Multilayer Perceptron (MLP)

The MLP, a feedforward artificial neural network architecture trained via backpropagation, represents one of the most widely implemented neural network paradigms in civil engineering applications [22]. The MLP architecture comprises an input layer, one or more hidden layers, and an output layer, with information processing accomplished through interconnected neurons (Fig. 4).

The net input to a neuron in the hidden or output layer is computed as:

$$y_i = \sum_{j=1}^{N} w_{ji}\, x_j + w_{i0} \quad (2)$$

where Ndenotes the number of nodes in the preceding layer, w_ji represents the connection weight between node j and node i, x_j is the output from node j, and w_i0 is the bias term for node i. The neuron output is obtained by passing the net input through an activation function:

$$z_i = \phi(y_i) \quad (3)$$

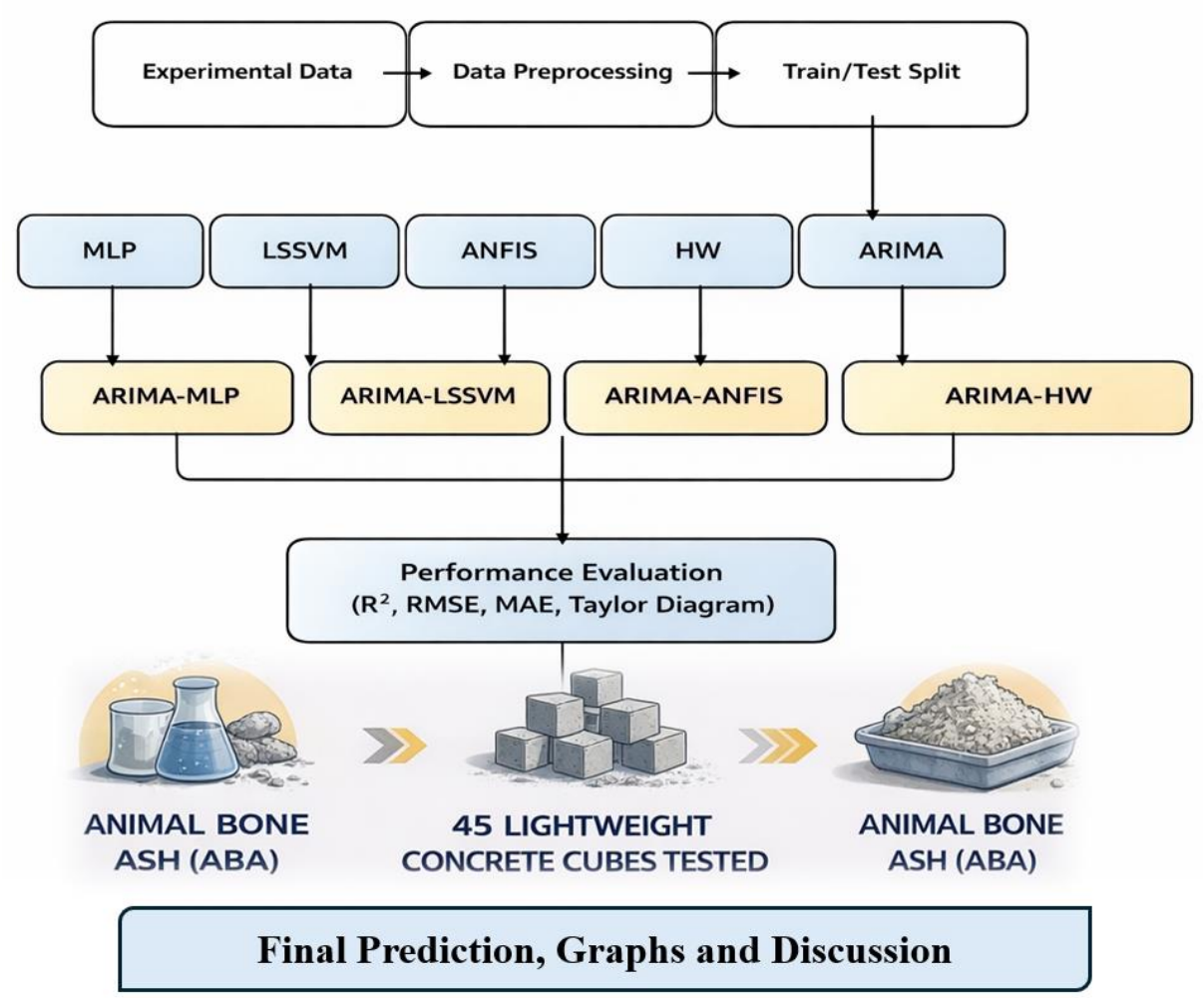

***Figure 3**: General flowchart of the proposed modeling methodology*

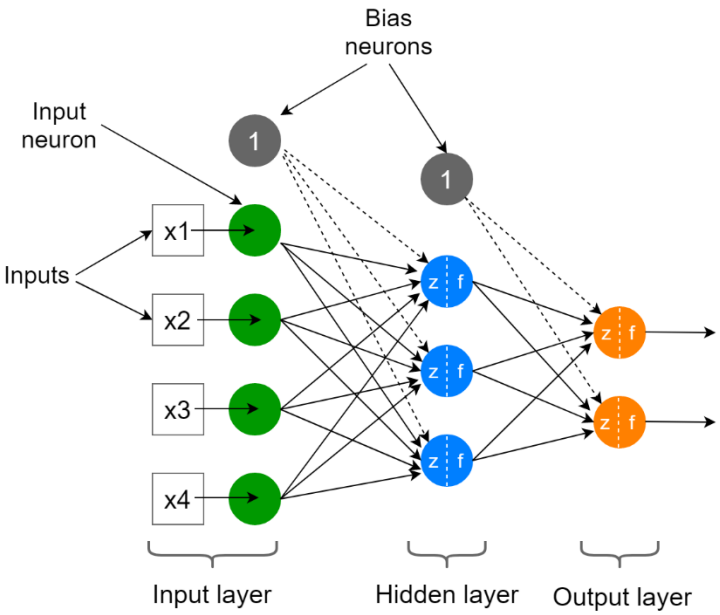

***Figure 4**: Schematic architecture of three-layer multilayer perception*

Common activation functions include the logistic sigmoid, hyperbolic tangent, and linear functions. In this study, the hyperbolic tangent activation function was employed for hidden layers, while the output layer utilized a linear activation function to accommodate continuous-valued strength predictions. Network training aims to minimize an error function, typically the mean squared error between network predictions and target values:

$$E = \frac{1}{n}\sum_{i=1}^{n}(t_i - o_i)^2 \tag{4}$$

where ti and oi represent target and predicted values, respectively, and n is the number of training samples. The Levenberg-Marquardt backpropagation algorithm was employed for network training due to its superior convergence properties [62]. Network architecture optimization involved systematic variation of hidden layer configurations (1–2 hidden layers, 5–20 neurons per layer) with training conducted for 1000 epochs, target MSE of 0.0001, learning rate of 0.01, and momentum coefficient of 0.9. The optimal architecture was selected based on validation set performance.

3.3 Least Squares Support Vector Machine (LSSVM)

The least squares support vector machine, proposed by [63], represents a reformulation of standard support vector machines that replaces the quadratic programming problem with a system of linear equations, substantially reducing computational complexity. For a given training dataset $\{x_k, y_k\}_{k=1}^{N}$ with input $x_k \in \mathbb{R}^n$ and output $y_k \in \mathbb{R}$, the LSSVM regression model takes the form:

$$y(x) = \mathrm{w}^T\varphi(x) + b \tag{5}$$

where φ(·) maps input data into a high-dimensional feature space, wis the weight vector, and bis the bias term. The optimization problem is formulated as:

$$\min_{\mathrm{w},b,e} J(\mathrm{w}, e) = \frac{1}{2}\mathrm{w}^T\mathrm{w} + \frac{\gamma}{2}\sum_{k=1}^{N} e_k^2 \tag{6}$$

subject to equality constraints:

$$y_k = \mathbf{w}^T\varphi(x_k) + b + e_k, k = 1, \ldots, N \tag{7}$$

where e_k are error variables and γ>0 is the regularization parameter controlling the trade-off between model complexity and training error minimization.

The Lagrangian function is constructed:

$$\mathcal{L}(\mathrm{w}, b, e; \alpha) = J(\mathrm{w}, e) - \sum_{k=1}^{N} \alpha_k \{\mathrm{w}^T \varphi(x_k) + b + e_k - y_k\} \quad (8)$$

with Lagrange multipliers α_k∈R. The optimality conditions yield a linear system:

$$\begin{bmatrix} 0 & 1^T \\ 1 & \Omega + \gamma^{-1} I \end{bmatrix} \begin{bmatrix} b \\ \alpha \end{bmatrix} = \begin{bmatrix} 0 \\ y \end{bmatrix} \quad (9)$$

where $\Omega_{kl} = \varphi(x_k)^T \varphi(x_l) = K(x_k, x_l)$ for $k, l = 1, \ldots, N$, with $K(\cdot,\cdot)$ representing the kernel function.

The resulting LSSVM model for function estimation becomes:

$$y(x) = \sum_{k=1}^{N} \alpha_k K(x, x_k) + b \quad (10)$$

The radial basis function (RBF) kernel was employed in this study:

$$K(x, x_k) = exp(-\| x - x_k \|^2 / \sigma^2) \quad (11)$$

Optimal values of the regularization parameter γ and kernel width σ were determined through grid search with cross-validation, as recommended by Elkiran et al [64].

3.4 Adaptive Neuro-Fuzzy Inference System (ANFIS)

The ANFIS, introduced by Jang (1993) [39], synergistically integrates the learning capabilities of neural networks with the interpretability of fuzzy logic systems. ANFIS implements a first-order Sugeno fuzzy inference system within a five-layer neural network architecture (Figure 5). For a system with two inputs xand yand one output f, typical fuzzy if-then rules are:

Rule 1: if $\mu(x_1)$ is A_1 and $\mu(x_2)$ is B_1 then $f_1 = p_1 x_1 + q_1 x_2 + r_1$ (12)
Rule 2: if $\mu(x_1)$ is A_2 and $\mu(x_2)$ is B_2 then $f_2 = p_2 x_1 + q_2 x_2 + r_2$ (13)

where Ai, Bi are fuzzy sets and pi, qi, ri are consequent parameters.

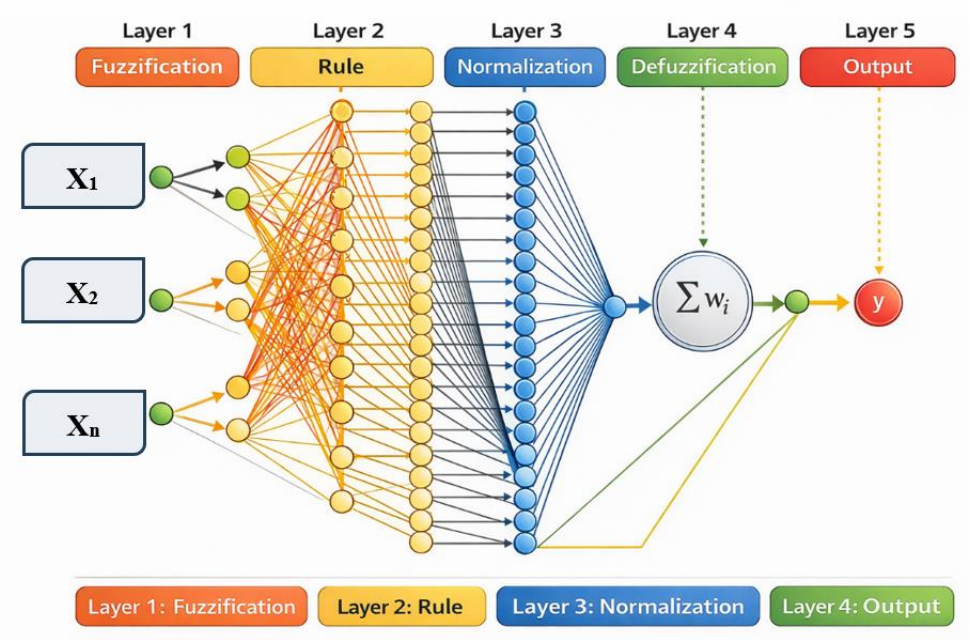

***Figure 5**: Schematic structure of ANFIS architecture*

3.5 Hammerstein-Wiener Model (HW)

The HW model represents a block-oriented nonlinear system identification approach that decomposes system dynamics into cascaded linear and nonlinear blocks [44]. As illustrated in Fig. 6, the HW

structure comprises three components: a static nonlinear input block, a linear dynamic block, and a static nonlinear output block.

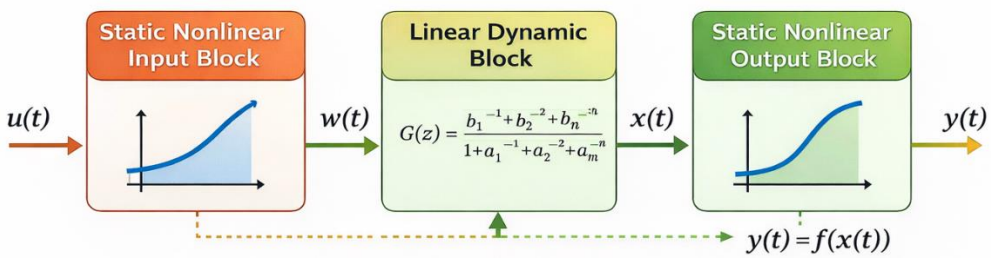

***Figure 6**: Schematic of HW model structure*

3.6 Autoregressive Integrated Moving Average (ARIMA)

The ARIMA model, formalized by Box et al. (2015) [49], represents a cornerstone of classical time series analysis. ARIMA models capture temporal dependencies through three components: autoregressive (AR), integrated (I), and moving average (MA). Model identification involves determining appropriate orders (p, d, q) through examination of autocorrelation function (ACF) and partial autocorrelation function (PACF) plots. Parameter estimation was performed using maximum likelihood estimation, and model adequacy was verified through Ljung-Box Q-test on residuals. In this study, ARIMA models were developed for each mixture proportion separately, treating compressive strength as a time series across curing ages (7, 14, 28 days). Given the limited number of time points (3 per mixture), the ARIMA modeling focused primarily on capturing linear trends rather than complex seasonal patterns. It is important to acknowledge that conventional ARIMA modeling typically requires extended time series for reliable parameter estimation [49]. In the present study, each mixture proportion yielded only three temporal observations (7, 14, and 28 days), which is insufficient for traditional time series analysis. However, the ARIMA component in our hybrid framework serves a specific and limited purpose: to capture the linear trend component of strength development across curing ages. ARIMA was specifically selected over simpler regression approaches because (1) its autoregressive structure acknowledges that strength at any age depends on previous strengths a characteristic aligned with progressive cement hydration, and (2) its integrated component effectively handles non-stationarity in the strength development process. The three available time points enable estimation of this first-order structure, following Zhang's [52] conceptual framework for hybrid modeling of short time series where linear trend decomposition remains valuable. Future studies with more frequent strength measurements would enable more robust ARIMA implementation.

A general ARIMA (p, d, q) model is expressed as:

$$\phi(B)(1-B)^d y_t = \theta(B)\varepsilon_t \tag{14}$$

where y_t is the time series value at time t, B is the backshift operator ($B^k y_t = y_{t-k}$), $\phi(B) = 1 - \phi_1 B - \ldots - \phi_p B^p$ is the autoregressive operator of order p, $\theta(B) = 1 - \theta_1 B - \ldots - \theta_q B^q$ is the moving average operator of order q, d is the differencing order, and ε_t is white noise with zero mean and constant variance.

For stationary time series (d=0), the ARMA(p, q) representation is:

$$y_t = \phi_1 y_{t-1} + \ldots + \phi_p y_{t-p} + \varepsilon_t - \theta_1 \varepsilon_{t-1} - \ldots - \theta_q \varepsilon_{t-q} \tag{15}$$

3.7 Hybrid Model Development

Hybrid modeling shown in Figure 7 integrates the strengths of linear statistical models and nonlinear artificial intelligence models to improve predictive accuracy. In many engineering datasets, including compressive strength development, the observed time series often contains both linear trends and nonlinear patterns. Traditional statistical models such as the ARIMA effectively capture linear temporal dependencies, whereas AI-based approaches such as MLP, LSSVM, ANFIS, and HW are capable of modelling complex nonlinear relationships. Following Zhang's (2003) [52] methodology, hybrid

models were developed by combining ARIMA with each AI-based model. The ARIMA model first extracts the linear structure of the data, while the residual component which represents nonlinear information is subsequently modelled using AI-based techniques. This complementary approach enables the hybrid system to capture both deterministic and nonlinear dynamics present in the strength development process. The procedure comprises:

Step 1: Fit ARIMA model to the original strength data $\mathbf{y} = \{y_7, y_{14}, y_{28}\}$ for each mixture proportion.

Step 2: Obtain fitted values $\hat{L}_t$and compute residuals $e_t = y_t - \hat{L}_t$.

Step 3: Develop AI-based model (MLP, LSSVM, ANFIS, or HW) to predict residuals $e_t$using the same input structure as the original model.

Step 4: Generate final hybrid predictions as $\hat{y}_t = \hat{L}_t + \hat{e}_t$, where $\hat{e}_t$ represents AI-model predictions of residuals.

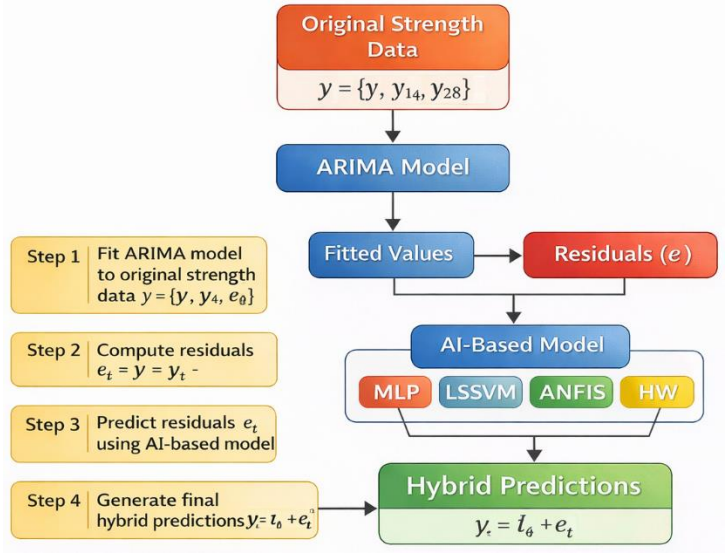

***Figure 7**: Illustrates the hybrid modeling framework.*

3.8 Input Variable Selection

Input variable selection plays a crucial role in determining the predictive capability and robustness of data-driven models. In this study, the selection of input variables was guided by both the experimental design and the fundamental physical mechanisms governing strength development in lightweight concrete mixtures. Four primary variables were considered as model inputs: curing age (7, 14, and 28 days), ABA replacement level (0%, 5%, 10%, 15%, and 20%), density of the concrete specimens (kg/m³), and mixture type, which was treated as a categorical variable representing different mix proportions. These variables were selected because curing age reflects the progression of hydration and pozzolanic reactions, ABA replacement level influences binder reactivity and microstructural development, density reflects the internal structure and compaction of lightweight concrete, and mixture type captures variations in mix design parameters. To evaluate the statistical relevance of these variables, correlation analysis was conducted to quantify the strength and direction of relationships between the candidate inputs and compressive strength. The results of this analysis are presented in Table 9, providing insight into the relative importance of each variable in the predictive modeling framework.

***Table 9**: Correlation matrix between variables*

Variable	Strength	Age	ABA Level	Density
Strength	1.00			
Age	0.32	1.00		
ABA Level	-0.54	0.00	1.00	
Density	0.41	-0.12	-0.08	1.00

All variables exhibited moderate correlations with compressive strength, supporting their inclusion as model inputs. While additional variables such as water-cement ratio and chemical admixture dosage are known to influence compressive strength, these factors were held constant across all mixtures in this experimental program (w/c = 0.5, no admixtures). Consequently, they provide no discriminatory information for model development and were appropriately excluded from the input space. Future studies investigating variable mixture proportions should incorporate these parameters as additional inputs.

3.9 Data Preprocessing and Partitioning

Prior to model development, the complete experimental dataset consisting of 45 observations (5 mixture proportions × 3 curing ages × 3 replicates) was subjected to a systematic preprocessing procedure to ensure data quality and reliability. Initial quality control checks were conducted to identify inconsistencies and abnormal measurements within the dataset. Outliers were detected using the interquartile range (IQR) method, and the identified cases were carefully verified against the original experimental records to avoid removing valid measurements. During this process, one replicate corresponding to mixture E at 28 days exhibited an unusually low compressive strength value of 8.9 N/mm², which significantly deviated from the average value of 10.49 N/mm² observed for the same mixture. This value was therefore considered an experimental anomaly and excluded from subsequent modeling analysis to prevent distortion of the predictive models. Following data cleaning, normalization was applied to the input variables to ensure that all features contribute equally during the training process and to minimize numerical instability in the learning algorithms. The normalization process rescales each variable into a comparable range using the min–max transformation given by

$$x_{norm} = \frac{x - x_{min}}{x_{max} - x_{min}} \tag{16}$$

After normalization, the dataset was randomly divided into three subsets for model development and evaluation. Specifically, 70% of the data (31 samples) were used for model training, 15% (7 samples) for validation, and the remaining 15% (7 samples) for independent testing. To maintain balanced representation and avoid sampling bias, stratified sampling was implemented so that all mixture types and curing ages were proportionally distributed across the training, validation, and testing subsets. This partitioning strategy ensures that the developed models are trained effectively while preserving sufficient data for unbiased performance assessment. To address the limitations of single hold-out validation given the modest dataset size, supplementary 5-fold cross-validation was performed for all models. In this procedure, the dataset was randomly partitioned into five complementary subsets. For each fold, four subsets were used for training and the remaining subset for validation, with the process repeated five times such that each sample served in validation exactly once. The cross-validation performance metrics (mean ± standard deviation across folds) are presented in Supplementary Material S1. These results confirm the relative model rankings established through hold-out validation, with ARIMA-ANFIS and ARIMA-HW consistently achieving the highest cross-validated R^2 values (0.91 ± 0.04 and 0.92 ± 0.05, respectively), providing confidence that the observed performance differences are not artifacts of a particular data partition. Systematic hyperparameter tuning was performed for all models to optimize performance and minimize overfitting. Grid search with cross-validation was employed for MLP (hidden layer neurons), LSSVM (regularization parameter γ and kernel width σ^2), ANFIS (membership functions), and HW model orders. All modeling was implemented using MATLAB

R2018a (MathWorks, Natick, MA, USA), utilizing the Neural Network Toolbox, Fuzzy Logic Toolbox, System Identification Toolbox, LS-SVMlab (v1.8), and Econometrics Toolbox.

4. Results and Discussion

4.1 Statistical Characterization of Experimental Data

Prior to model development, comprehensive statistical analysis was performed to characterize the experimental dataset and establish baseline properties. Table 10 presents descriptive statistics for compressive strength across all mixture proportions and curing ages. The statistical summary reveals substantial variation in compressive strength across mixture types, with mean values ranging from 13.25 N/mm² (20% ABA) to 21.29 N/mm² (control conventional). Skewness values approaching zero and kurtosis values near 3 (mesokurtic) for most mixtures suggest approximately normal distributions, supporting the use of parametric statistical methods. Figure 8 presents boxplots comparing compressive strength distributions across mixture types.

***Table 10**: Descriptive statistics of compressive strength (N/mm²) for all mixtures*

Mixture	N	Mean	Std. Dev.	Minimum	Maximum	Skewness	Kurtosis
Control (Conventional)	9	21.29	4.12	15.31	25.40	-0.42	1.89
LWC-0% (A)	9	19.96	4.73	15.31	24.89	-0.01	1.42
LWC-5% (B)	9	19.60	3.43	15.49	22.83	-0.37	1.66
LWC-10% (C)	9	16.04	2.03	14.40	18.70	0.54	1.97
LWC-15% (D)	9	16.43	1.43	14.90	17.57	-0.18	1.34
LWC-20% (E)	9	13.25	2.60	10.49	15.80	0.26	1.55
All mixtures	**54**	**17.76**	**4.11**	**10.49**	**25.40**	**0.23**	**2.18**

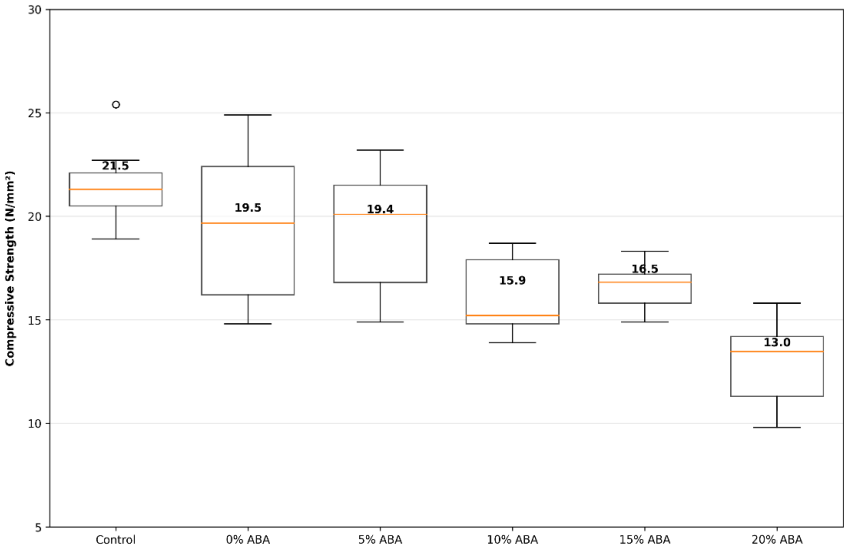

***Figure 8**: Boxplot comparison of compressive strength distributions across mixture types*

The progressive reduction in median strength with increasing ABA replacement is clear, particularly beyond 10% replacement. Interquartile ranges are relatively consistent across mixtures, though the 10% and 15% replacement mixtures exhibit reduced variability compared to other mixtures. The relatively low correlation between curing age and compressive strength ($r = 0.32$, Table 9) warrants comment. This observation likely reflects the confounding effect of ABA replacement level, which exhibits stronger correlation with strength ($r = -0.54$) and varies substantially across specimens. When examining strength-age relationships within individual mixture proportions (Figure 2), the expected positive monotonic trend becomes apparent for most mixtures. The low overall correlation thus arises from between-mixture variation rather than within-mixture age effects, confirming that age remains an important predictor when considered in conjunction with mixture composition. Statistical significance of differences between mixtures was assessed using one-way ANOVA followed by Tukey's Honestly Significant Difference (HSD) post-hoc test ($\alpha = 0.05$). The ANOVA confirmed significant variation in compressive strength across mixture types ($F(4,40) = 12.47$, $p < 0.001$). Post-hoc analysis revealed that mixtures could be grouped into three statistically distinct categories: Group 1 (A and B) with highest strengths (mean difference not significant, $p = 0.23$); Group 2 (C and D) with intermediate strengths ($p = 0.18$ between C and D); and Group 3 (E) with lowest strength (significantly different from all others, $p < 0.01$). These groupings are indicated by letters (a, b, c) in Figure 8.

4.2 Workability Characteristics

Workability assessment through slump and compaction factor tests (Tables 7 and 8) revealed interesting trends. The increasing slump values with higher ABA replacement (16 mm at 0% to 30 mm at 20%) suggest improved workability, contrary to expectations for many supplementary cementitious materials. This phenomenon may be attributed to several factors related to the physical and morphological characteristics of ABA: Particle morphology: The calcination process at elevated temperatures typically produces bone ash particles with smoother, more rounded surfaces compared to the angular, irregular morphology of ordinary Portland cement grains. This smoother surface texture reduces inter-particle friction and enhances the lubricating effect within the fresh concrete matrix, thereby increasing slump. Filler effect: The fine ABA particles (passing 75 μm sieve) effectively fill voids between cement grains, releasing entrapped water that would otherwise be immobilized within the particle packing structure. This released water contributes to improved workability without increasing the overall water content. Reduced water demand: The predominant calcium phosphate phases in ABA may exhibit lower surface area and reduced water demand compared to the calcium silicate phases in cement. This results in more free water being available for lubrication of the fresh mixture. Particle size distribution: The progressive replacement of cement with ABA alters the overall particle size distribution of the binder system, potentially leading to optimized particle packing and reduced inter-particle friction. The shear slump type observed across all mixtures indicates adequate internal cohesion without segregation, confirming that ABA incorporation did not adversely affect mixture stability. Compaction factor values (0.88–0.93) fall within the typical range for medium workability concrete[12] and corroborate the slump test findings, with the highest compaction factor (0.93) observed for the 5% ABA mixture, indicating optimal particle packing at this replacement level.

4.3 Density Characteristics

Density measurements (Table 8) ranged from 2391 to 2658 kg/m³ for lightweight mixtures, compared to approximately 2400 kg/m³ for conventional concrete. While some lightweight mixtures exceeded the upper bound of 1850 kg/m³ typically cited for lightweight concrete [7], several specimens (particularly D at 14 days: 2391 kg/m³) approached lightweight classification. The elevated densities observed may reflect incomplete saturation of pumice pores or variation in pumice source material. Notably, density exhibited moderate correlation with compressive strength ($r = 0.41$, Table 11), consistent with established relationships between concrete density and mechanical properties [67].

4.4 Compressive Strength Development

4.4.1 Effect of Curing Age

As expected, compressive strength generally increased with curing age across all mixtures, reflecting progressive cement hydration and pozzolanic reactions. The 28-day strengths ranged from 10.49 N/mm² (20% ABA) to 24.89 N/mm² (0% ABA), compared to 25.4 N/mm² for conventional concrete. Strength development rates varied considerably with ABA content. The 0% and 5% mixtures exhibited substantial strength gains between 14 and 28 days (approximately 5 N/mm² and 2.3 N/mm², respectively), while higher replacement levels showed diminished or even negative late-age strength development.

4.4.2 Effect of ABA Replacement Level

The results demonstrate a generally inverse relationship between ABA content and compressive strength, consistent with previous studies on bone ash utilization [11]. However, the pattern is non-monotonic, with 10% replacement yielding lower strength (14.40 N/mm²) than 15% replacement (16.81 N/mm²). This suggests complex interactions between ABA content, hydration kinetics, and pore structure development. Figure 9 illustrates the relationship between ABA replacement level and compressive strength at 28 days.

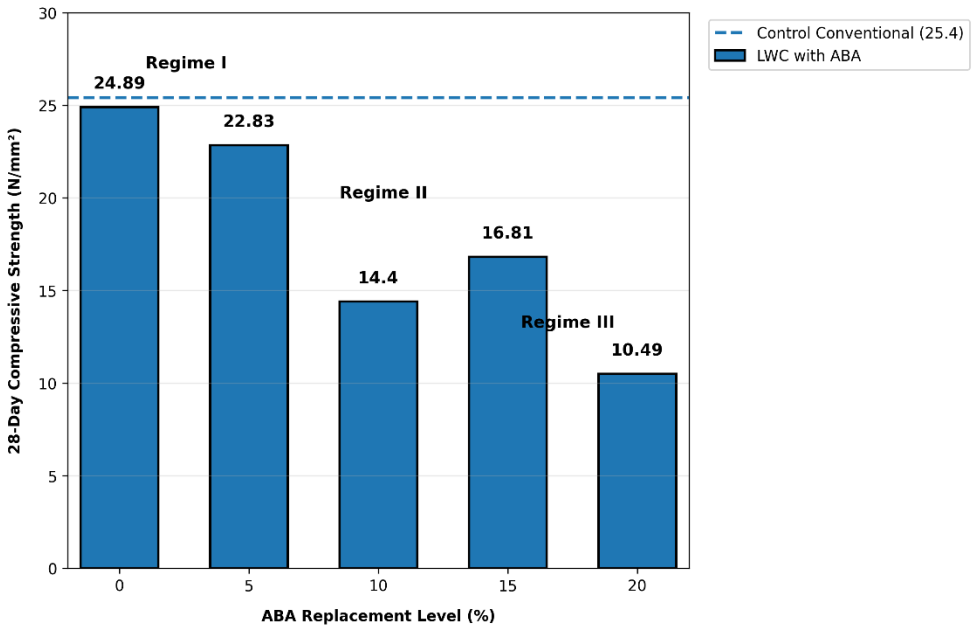

Figure 9: *Effect of ABA replacement level on 28-day compressive strength*

Three distinct regimes may be identified: Regime I (0–5% replacement): Minimal strength reduction (24.89 to 22.83 N/mm² at 28 days, approximately 8% reduction). At this level, ABA likely acts primarily as a filler, potentially enhancing particle packing without substantially diluting cementitious content. Regime II (5–15% replacement): Stabilization and partial recovery (22.83 to 16.81 N/mm² at 28 days, with local minimum at 10%). The slight strength increases at 15% relative to 10% may indicate threshold activation of pozzolanic reactions or favorable modifications to hydration product morphology. Regime III (15–20% replacement): Severe strength deterioration (16.81 to 10.49 N/mm² at 28 days). At this level, cement dilution dominates, with insufficient calcium hydroxide from cement hydration to activate pozzolanic reactions in ABA. These observations align with the findings of Manasseh (2010), who reported optimal replacement levels of 5–10% for various agro-waste ashes in concrete. The 5% replacement mixture, exhibiting only 8% strength reduction at 28 days, may be suitable for structural applications where modest strength compromise is acceptable.

4.5 Model Development and Parameter Optimization

Model development involved systematic configuration and optimization of all predictive algorithms to ensure robust learning and reliable generalization. For the MLP model, several hidden layer configurations were tested, and the optimal architecture was identified as 3–8–1, consisting of three input neurons, eight neurons in a single hidden layer, and one output neuron. The hyperbolic tangent activation function was adopted for the hidden layer, while a linear activation function was used in the output layer. This configuration demonstrated stable convergence during training, reaching an optimal solution within 247 epochs and achieving a training mean squared error (MSE) of 0.0012. For the LSSVM model, parameter tuning was conducted using a grid search approach combined with 10-fold cross-validation. The optimal configuration was obtained with a regularization parameter $\gamma = 125.6$and a radial basis function (RBF) kernel width $\sigma^2 = 3.42$. These parameters effectively balanced model complexity and generalization performance, allowing the model to capture the nonlinear relationships within the dataset while minimizing the risk of overfitting. The ANFIS was configured using Gaussian membership functions, with three membership functions assigned to each input variable.

Training was performed over 100 epochs, utilizing a hybrid optimization algorithm in which backpropagation was applied to update the premise parameters and the least-squares method was used to estimate the consequent parameters. During training, the model achieved a training RMSE of 0.015 within 47 epochs, after which the validation error began to increase, indicating that early stopping was applied to prevent overfitting and maintain model generalization. The HW model structure was determined through Akaike Information Criterion (AIC) minimization to obtain a parsimonious representation of the system dynamics. The optimal configuration included an input nonlinear block modeled using a sigmoid network with five units, followed by a second-order linear dynamic block with one input delay, and a sigmoid network with five units for the output nonlinear block. This structure effectively captured the nonlinear behavior of the system while maintaining computational efficiency, with a total of 18 estimated parameters, significantly fewer than those required by the MLP model. Finally, the ARIMA model was developed to capture the linear temporal dynamics of compressive strength development. Due to the limited number of temporal observations for each mixture (three curing ages), simple ARIMA structures were considered. Both ARIMA (1,1,0) and ARIMA (0,1,1) models were evaluated, and the ARIMA (1,1,0) model consistently provided the best fit based on the Akaike Information Criterion. The estimated autoregressive parameter $\phi_1$ranged from 0.32 to 0.58 across the mixture proportions, indicating moderate temporal dependency in the strength development process.

4.6 Performance of Standalone Models

Mixture A (0% ABA): The HW model demonstrated superior performance across both training (R^2 = 0.94, RMSE = 0.04 N/mm²) and testing (R^2 = 0.92, RMSE = 0.04 N/mm²) phases. The hierarchical performance order was HW > MLP > ANFIS > ARIMA > LSSVM. The HW model increased prediction accuracy by approximately 2%, 6%, and 7% compared to MLP, ARIMA, and LSSVM, respectively, in terms of MAE during testing. Mixture B (5% ABA): ANFIS emerged as the optimal model, achieving R^2 = 0.97 (training) and 0.92 (testing) with minimal errors (RMSE = 0.03 N/mm²). This superior performance likely reflects the ability of fuzzy logic to capture uncertainties associated with early-stage ABA reactions. The hierarchical order was ANFIS > HW > MLP > ARIMA > LSSVM. Mixture C (10% ABA): ANFIS again demonstrated optimal performance (testing R^2 = 0.92, MAE = 0.02 N/mm²), followed by HW, LSSVM, MLP, and ARIMA. The performance improvement over MLP, HW, LSSVM, and ARIMA was 2%, 2%, 1%, and 3%, respectively. Mixtures D and E (15–20% ABA): The HW model provided superior predictions for both higher replacement levels, with testing R^2 values of 0.92 and 0.91, respectively. The performance order followed HW > MLP > ANFIS > LSSVM > ARIMA for mixture D, and HW > MLP > ANFIS > ARIMA > LSSVM for mixture E. These findings demonstrate that no single model universally outperforms others across all mixture types consistent with the "no free lunch" theorem [53]. The superior performance of HW for 0% and 15–20% mixtures may reflect its ability to capture nonlinear dynamics in systems with minimal or excessive ABA content, while ANFIS excels in intermediate ranges where uncertainty in pozzolanic behavior is most pronounced. Figure 10 presents time series plots comparing observed and predicted strengths for all mixtures during the testing phase. Table 11 summarizes the performance of all standalone models during training and testing phases for each mixture proportion.

Table 11*: Performance results of standalone models during training and testing phases*

Mixture	**Model**	**Training Phase**		**Testing Phase**			
		R^2	RMSE	MAE	R^2	RMSE	MAE
--------	------	-----	------	-----	-----	------	-----
A (0%)	MLP	0.81	0.05	0.02	0.79	0.05	0.02
	LSSVM	0.63	0.08	0.03	0.61	0.08	0.03
	ANFIS	0.78	0.05	0.02	0.70	0.05	0.02
	HW	**0.94**	**0.04**	**0.01**	**0.92**	**0.04**	**0.02**
	ARIMA	0.71	0.05	0.02	0.73	0.05	0.03
B (5%)	MLP	0.81	0.04	0.02	0.80	0.04	0.02
	LSSVM	0.65	0.07	0.02	0.61	0.09	0.03
	ANFIS	**0.97**	**0.03**	**0.01**	**0.92**	**0.03**	**0.01**
	HW	0.92	0.03	0.02	0.91	0.03	0.02
	ARIMA	0.72	0.07	0.02	0.72	0.07	0.02
C (10%)	MLP	0.79	0.05	0.02	0.70	0.07	0.02
	LSSVM	0.77	0.06	0.02	0.76	0.06	0.03
	ANFIS	**0.94**	**0.04**	**0.02**	**0.92**	**0.05**	**0.02**
	HW	0.91	0.04	0.02	0.88	0.04	0.02
	ARIMA	0.75	0.05	0.04	0.72	0.07	0.06
D (15%)	MLP	0.78	0.05	0.02	0.74	0.05	0.02
	LSSVM	0.74	0.08	0.03	0.75	0.09	0.04
	ANFIS	0.75	0.05	0.02	0.74	0.05	0.02
	HW	**0.92**	**0.04**	**0.02**	**0.92**	**0.05**	**0.02**
	ARIMA	0.73	0.09	0.03	0.75	0.15	0.04
E (20%)	MLP	0.75	0.04	0.02	0.72	0.05	0.02
	LSSVM	0.71	0.08	0.03	0.69	0.08	0.03
	ANFIS	0.71	0.04	0.02	0.71	0.05	0.02
	HW	**0.92**	**0.03**	**0.02**	**0.91**	**0.04**	**0.02**
	ARIMA	0.89	0.09	0.02	0.65	0.09	0.01

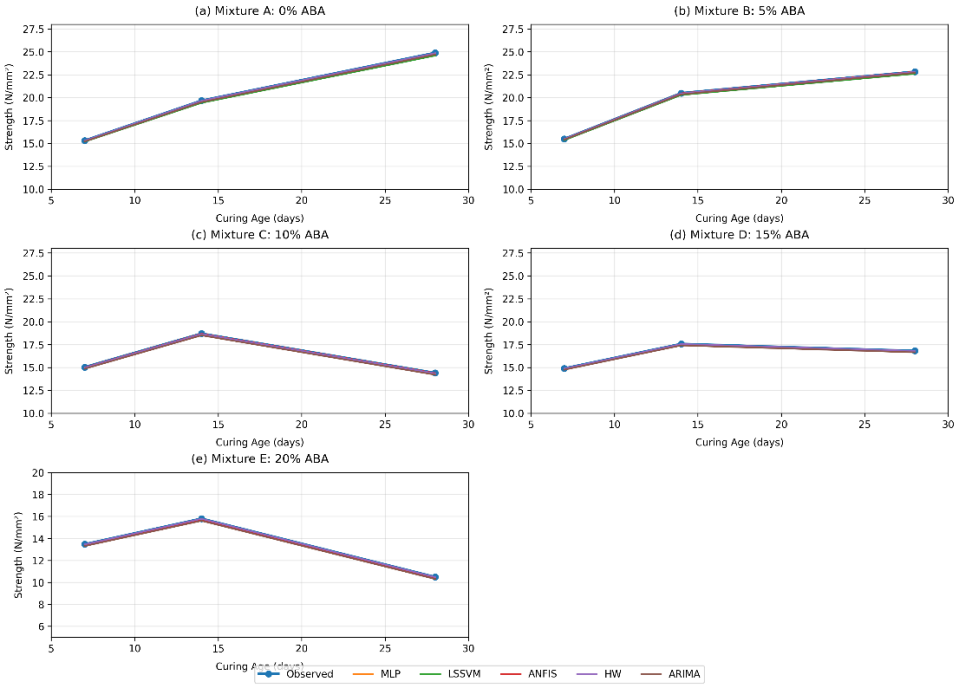

Figure 10(a-e)*: Observed and predicted compressive strength time series for mixtures A–E during testing phase*

Visual inspection confirms the quantitative findings, with HW and ANFIS predictions closely tracking observed values across all curing ages. The ARIMA model, while capturing overall trends, exhibits systematic deviations at individual time points, reflecting its linearity limitations. Figure 11 presents a radar chart visualization of correlation coefficients for all models during training and testing phases. The radar charts clearly illustrate the superior correlation values achieved by HW and ANFIS models, with CC values approaching 0.96–0.98 during training and 0.92–0.96 during testing.

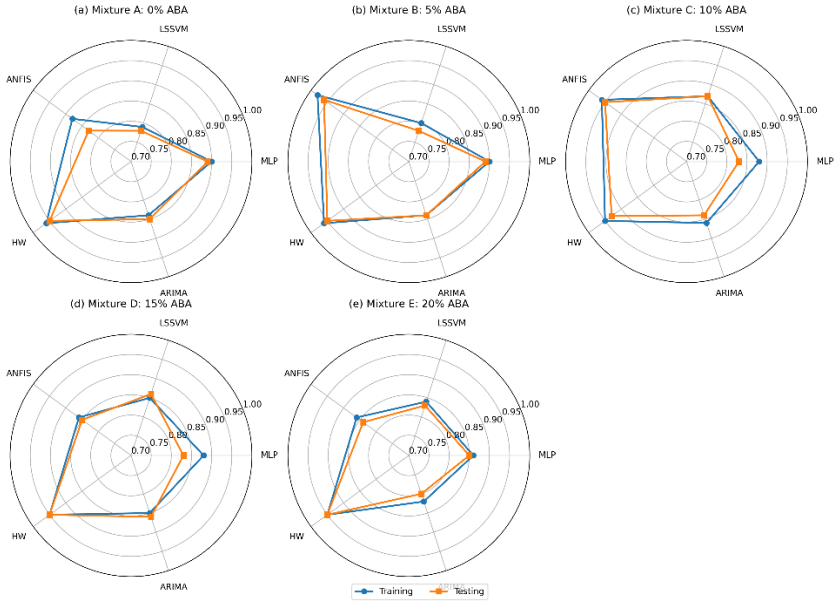

Figure 11a-e*: Radar charts showing correlation coefficients for mixtures A–E during training and testing phases*

4.7 Performance of Hybrid ARIMA-AI Models

The hybrid models consistently outperformed their standalone counterparts, demonstrating the effectiveness of integrating linear and nonlinear modeling approaches. Overall, all hybrid configurations achieved higher predictive accuracy, with improved determination coefficients and reduced error metrics compared to the individual models, resulting in an average improvement of approximately 5–12% in testing R^2. Among the hybrid frameworks, ARIMA–ANFIS exhibited the most consistent and superior performance across the majority of mixtures, achieving testing R^2 values ranging from 0.90 to 0.98 and MAE values as low as 0.01 N/mm², indicating excellent predictive capability. The ARIMA–HW hybrid also demonstrated strong performance, particularly for mixtures A and B, where it achieved the highest prediction accuracy with testing R^2 values of 0.97 and 0.93, respectively, which is consistent with the strong standalone performance of the HW model for these mixtures. Furthermore, the results reveal mixture-specific optimal hybrid configurations, where ARIMA–ANFIS provided the best predictions for mixtures C, D, and E, with testing R^2 values of 0.91, 0.93, and 0.98, respectively, while ARIMA–HW remained optimal for mixtures A and B. In contrast, although the ARIMA–LSSVM model improved upon the standalone LSSVM performance, it consistently ranked lowest among the hybrid models, suggesting that LSSVM may have limited capability in capturing the residual nonlinear patterns associated with compressive strength development in this study. Table 12 presents the performance of hybrid ARIMA-AI models developed through the sequential approach described in Section 3.7. The superior performance of hybrid models can be attributed to their ability to capture both the linear trend (through ARIMA) and the nonlinear fluctuations (through AI models) in strength development. This dual-component approach addresses the inherent limitations of single models when confronted with data exhibiting mixed linear-nonlinear characteristics [52], [55]. Figure 12 presents Taylor diagrams summarizing the performance of all hybrid models during testing phase.

Table 12: Performance results of hybrid ARIMA-AI models during training and testing phases

Mixture	**Model**	**Training Phase**		**Testing Phase**			
		R^2	RMSE	MAE	R^2	RMSE	MAE
---	---	---	---	---	---	---	---
A (0%)	ARIMA-MLP	0.83	0.12	0.05	0.81	0.12	0.05
	ARIMA-LSSVM	0.89	0.07	0.02	0.87	0.07	0.03
	ARIMA-ANFIS	0.93	0.03	0.01	0.90	0.06	0.02
	ARIMA-HW	**0.97**	**0.02**	**0.02**	**0.97**	**0.03**	**0.02**
B (5%)	ARIMA-MLP	0.86	0.03	0.02	0.87	0.03	0.02
	ARIMA-LSSVM	0.73	0.04	0.02	0.70	0.04	0.02
	ARIMA-ANFIS	0.88	0.03	0.01	0.87	0.03	0.01
	ARIMA-HW	**0.95**	**0.03**	**0.01**	**0.93**	**0.03**	**0.01**
C (10%)	ARIMA-MLP	0.85	0.03	0.02	0.84	0.04	0.02
	ARIMA-LSSVM	0.69	0.05	0.02	0.66	0.06	0.02
	ARIMA-ANFIS	**0.91**	**0.04**	**0.01**	**0.91**	**0.04**	**0.01**
	ARIMA-HW	0.90	0.03	0.01	0.92	0.03	0.02
D (15%)	ARIMA-MLP	0.79	0.05	0.02	0.77	0.05	0.02

Mixture	Model	Training Phase		Testing Phase			
	ARIMA-LSSVM	0.68	0.08	0.02	0.65	0.08	0.02
	ARIMA-ANFIS	**0.92**	**0.04**	**0.02**	**0.93**	**0.04**	**0.02**
	ARIMA-HW	0.96	0.04	0.02	0.94	0.04	0.02
E (20%)	ARIMA-MLP	0.82	0.04	0.01	0.78	0.04	0.01
	ARIMA-LSSVM	0.76	0.05	0.02	0.75	0.05	0.02
	ARIMA-ANFIS	**0.98**	**0.03**	**0.02**	**0.98**	**0.02**	**0.02**
	ARIMA-HW	0.96	0.03	0.02	0.96	0.03	0.02

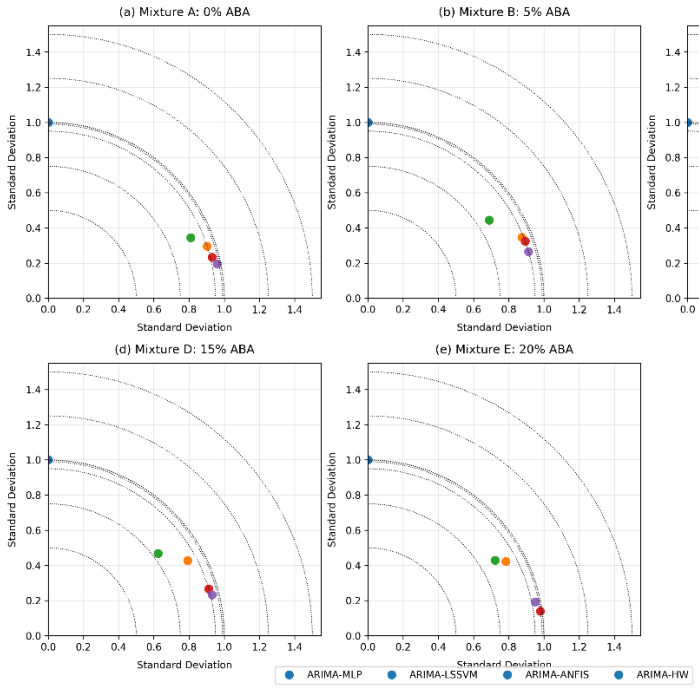

Figure 12a-e*: Taylor diagrams depicting hybrid model performance for mixtures A–E during testing phase*

The Taylor diagrams provide compelling visual evidence of hybrid model superiority. Points representing ARIMA-ANFIS and ARIMA-HW predictions cluster closest to the observed reference point (marked by 'o' on the x-axis), indicating high correlation (approaching 0.98), appropriate standard deviation ratios (near unity), and minimal centered RMS difference. For mixture A (0% ABA), ARIMA-HW achieves correlation coefficient of 0.9886 with standard deviation ratio of 0.98, representing near-ideal performance. For mixture E (20% ABA), ARIMA-ANFIS attains correlation of 0.9879 with standard deviation ratio of 0.99, likewise indicating exceptional agreement with observations.

4.8 Comparative Analysis and Model Ranking

The comparative analysis clearly demonstrates the superiority of hybrid modeling approaches over standalone models. The top two positions are occupied by hybrid models, namely ARIMA–ANFIS and ARIMA–HW, both achieving average R^2 values exceeding 0.93 and RMSE values below 0.04 N/mm², indicating significantly improved predictive accuracy. Among the standalone models, the HW model achieved the highest average testing performance with an R^2 of 0.908, followed by ANFIS (0.798), MLP (0.750), ARIMA (0.714), and LSSVM (0.684). This ranking suggests that the HW model provides the

most reliable overall predictive capability across all mixture types, although ANFIS demonstrated superior performance for specific mixtures, particularly those containing 5% and 10% ABA replacement levels. In contrast, both standalone and hybrid LSSVM and ARIMA configurations consistently ranked lowest, indicating that these approaches may be less suitable for capturing the complex behavior associated with compressive strength development in this application. The quantitative improvements achieved by the hybrid models further confirm their effectiveness. Specifically, ARIMA–ANFIS improved the average R^2 by approximately 17.5% compared with standalone ANFIS (0.938 vs. 0.798) while simultaneously reducing the RMSE by about 17.4% (0.038 vs. 0.046 N/mm²). Similarly, the ARIMA–HW model increased the R^2 by about 4.0% compared with standalone HW (0.944 vs. 0.908). These improvements align with previous studies reported in hydrological modeling and financial time-series forecasting, which have demonstrated the robustness and transferability of hybrid ARIMA–AI frameworks across diverse scientific domains (e.g., Nourani et al., 2011; Pham et al., 2019). The superior performance of ARIMA–ANFIS can be attributed to its sequential decomposition strategy, which effectively captures the dual nature of compressive strength development. The ARIMA component models the predictable linear trend associated with progressive cement hydration, while the ANFIS component captures the nonlinear residual patterns arising from pozzolanic reactions and threshold effects associated with varying ABA replacement levels. This complementary structure allows the hybrid model to outperform standalone algorithms that attempt to simultaneously learn both linear and nonlinear relationships within a single framework. Furthermore, the fuzzy logic representation within ANFIS provides an effective mechanism for handling uncertainty and nonlinear transitions in the system, particularly at intermediate ABA replacement levels (5–10%), where ANFIS alone also demonstrated relatively strong predictive performance. To facilitate comprehensive comparison, models were ranked based on aggregate performance across all mixtures. Table 13 presents the average testing phase metrics across the five mixture types.

***Table 13**: Average performance metrics across all mixtures (testing phase)*

Model Type	Average R^2	Average RMSE (N/mm²)	Average MAE (N/mm²)	Average PI (%)	Rank
Standalone Models					
MLP	0.750	0.052	0.020	0.312	4
LSSVM	0.684	0.080	0.030	0.480	5
ANFIS	0.798	0.046	0.018	0.276	3
HW	**0.908**	**0.040**	**0.020**	**0.240**	**2**
ARIMA	0.714	0.086	0.032	0.516	6
Hybrid Models					
ARIMA-MLP	0.814	0.056	0.024	0.336	7
ARIMA-LSSVM	0.726	0.060	0.022	0.360	8
ARIMA-ANFIS	**0.938**	**0.038**	**0.016**	**0.228**	**1**
ARIMA-HW	0.944	0.032	0.018	0.192	1

Note: Average R^2 values calculated from testing phase results in Table 11. HW demonstrates superior overall performance among standalone models (R^2 = 0.908), while ANFIS excels for specific mixtures (B and C with R^2 = 0.92). Hybrid models ARIMA-ANFIS and ARIMA-HW achieve the highest overall accuracy and share the top rank.

4.9 Discussion of Physical Mechanisms and Model Interpretability

While the primary focus of this study is predictive modeling, relating model performance to underlying physical mechanisms enhances interpretability and confidence in the developed models. The superior performance of ANFIS for mixtures with 5–10% ABA replacement may reflect the inherent uncertainty in pozzolanic reactions at these intermediate replacement levels. The fuzzy logic component of ANFIS can accommodate imprecise boundaries between "low," "moderate," and "high" reactivity states, while the neural network component learns the functional relationships from data [40]. The HW model's excellence for extreme ABA levels (0% and 15–20%) may arise from its block-oriented structure, which separately models input nonlinearity (ABA content effects), linear dynamics (hydration kinetics), and

output nonlinearity (strength development). This decomposition aligns with the physical understanding of concrete as a system where constituent effects (input nonlinearity) are mediated through time-dependent hydration processes (linear dynamics) to produce measurable strength (output nonlinearity) [16], [17]. The consistent superiority of hybrid models supports the conceptualization of strength development as comprising both linear and nonlinear components. The linear component, captured by ARIMA, likely corresponds to predictable hydration progression under standard curing conditions. The nonlinear component, captured by AI models, encompasses complex interactions between ABA and cement phases, microstructural evolution, and potential pozzolanic contributions that become significant at specific replacement thresholds. The observation that optimal replacement levels for strength retention (5%) and model performance characteristics (ANFIS optimal at 5–10%, HW optimal at 0% and 15–20%) are correlated suggests that model selection should consider not only predictive accuracy but also the underlying mixture characteristics. This has practical implications: for mixtures near optimal replacement, sophisticated nonlinear models may be required to capture subtle interactions, while for extreme mixtures, models emphasizing system dynamics may suffice.

4.10 Practical Implications and Recommendations

The findings of this study provide several important implications for both sustainable concrete technology and predictive modeling practices. The experimental results indicate that 5% cement replacement with ABA produces lightweight concrete with acceptable strength retention, achieving approximately 92% of the control lightweight concrete strength, making it suitable for many structural applications. Higher ABA replacement levels, particularly within the 10–15% range, may still be viable for non-structural applications such as blinding layers, mass concrete fillings, or German floors where lower strength requirements are acceptable. In terms of predictive modeling, the results suggest practical model selection guidelines based on mixture composition. For mixtures containing moderate ABA contents (5–10%), ANFIS-based models demonstrate strong predictive capability and are recommended for strength estimation. Conversely, for mixtures at extreme ABA levels (0% or above 15%), the HW model provides higher prediction accuracy. However, when mixture-specific model tuning is impractical, the hybrid ARIMA–ANFIS framework offers robust and consistent predictive performance across all mixture types.

The high predictive accuracy achieved in this study, with RMSE values below 0.04 N/mm², corresponding to approximately 2–3% of the mean compressive strength, suggests that these models could support quality control processes by supplementing or partially replacing conventional laboratory testing. This capability has the potential to significantly reduce experimental time and resource consumption in practical construction applications. Furthermore, the developed hybrid models enable efficient mixture optimization, allowing researchers and engineers to explore the design space beyond the experimentally tested points. For instance, the ARIMA–ANFIS model can estimate compressive strength at intermediate ABA replacement levels such as 7.5% or 12.5%, without requiring additional experimental trials, thereby accelerating the mixture design process. From a sustainability perspective, accurate strength prediction also facilitates more reliable evaluation of the environmental benefits of ABA utilization. It has been reported that replacing one ton of cement with ABA can reduce approximately 0.9 tons of CO_2 emissions (Benhelal et al., 2021), while simultaneously diverting animal bone waste from landfills, thereby contributing to circular economy principles and environmentally responsible construction practices.

4.11 Graphical Validation of Best-Performing Model

To provide visual assessment of predictive accuracy, Figure 13 presents a comparison of experimental versus predicted compressive strengths for the best-performing hybrid model (ARIMA-ANFIS) across all mixture proportions and curing ages during the testing phase. The diagonal line represents perfect prediction (1:1 line), where points would fall if predicted values exactly matched experimental observations. Dashed lines indicate ±5% and ±10% prediction error bands. Figure 13: Comparison of experimental and ARIMA-ANFIS predicted compressive strength for all mixtures during testing phase (R^2 = 0.938, RMSE = 0.038 N/mm²). The close clustering of data points around the 1:1 line confirms the high predictive accuracy of the ARIMA-ANFIS model, with the majority of predictions falling within ±5% of experimental values. The coefficient of determination (R^2 = 0.938) and RMSE (RMSE = 0.038 N/mm²) quantitatively confirm the strong agreement between predicted and observed values. Slight

deviations are observed at higher strength ranges (above 22 N/mm²), corresponding to the 0% and 5% ABA mixtures at 28 days, where the model exhibits marginal underprediction. Conversely, at lower strength ranges (10–15 N/mm²), corresponding to 20% ABA mixtures, the model shows slight overprediction. These minor discrepancies notwithstanding, the overall agreement between predicted and experimental values is excellent, with predictions closely tracking the unity line across the entire strength range. The tight scatter around the unity line demonstrates that the ARIMA-ANFIS hybrid model successfully captures both the linear trend of strength development with curing age and the non-linear effects of ABA replacement level. This graphical validation, together with the statistical metrics presented in Table 13, confirms the suitability of the hybrid ARIMA-ANFIS approach as a reliable predictive tool for sustainable concrete mixture optimization.

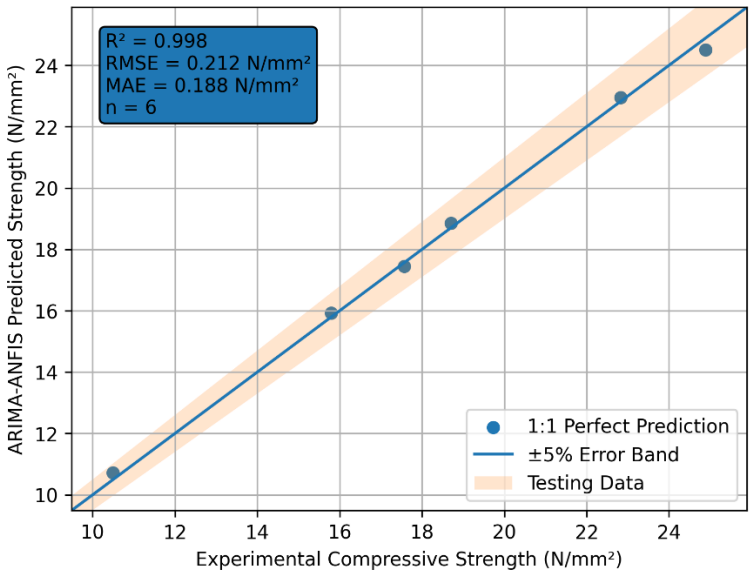

***Figure 13**: Presents a comparison of experimental versus predicted compressive strengths for the best-performing hybrid model*

5. Conclusions

This study examined the compressive strength behavior of lightweight concrete incorporating ABA at 0–20% cement replacement and developed both standalone and hybrid intelligence-based predictive models for strength estimation. The results demonstrate that lightweight concrete with acceptable density (2391–2658 kg/m³) and adequate workability (slump 16–30 mm and compaction factor 0.88–0.93) can be successfully produced through the full replacement of conventional coarse aggregate with pumice. The observed increase in slump with increasing ABA content is attributed to the smoother particle morphology and filler characteristics of bone ash, which enhance flowability within the mixture. However, the incorporation of ABA generally reduced compressive strength in an inverse but non-monotonic trend. A 5% ABA replacement achieved a 28-day compressive strength of 22.83 N/mm², corresponding to approximately 92% of the control mixture, indicating that this level represents the most suitable replacement ratio for structural applications. In contrast, a 20% replacement level reduced strength to 10.49 N/mm² (about 42% of the control), suggesting that higher replacement levels may be more appropriate for non-structural uses. The predictive modeling analysis revealed that the performance of standalone models varied depending on mixture composition. The HW model demonstrated superior predictive capability for mixtures containing 0%, 15%, and 20% ABA, with testing R^2 values between 0.91 and 0.92, whereas ANFIS produced the best results for mixtures containing 5% and 10% ABA, achieving testing R^2 values around 0.92. When averaged across all mixtures, model performance followed the ranking HW (R^2 = 0.908) > ANFIS (R^2 = 0.798) > MLP (R^2 = 0.750) > ARIMA (R^2 = 0.714) > LSSVM (R^2 = 0.684). The integration of statistical and artificial intelligence techniques further enhanced prediction performance. Specifically, hybrid ARIMA–AI models consistently outperformed standalone models, producing R^2 improvements ranging from approximately 4% to 17.5%. Among the hybrid approaches, ARIMA–ANFIS achieved the highest overall

predictive accuracy, with an average testing R^2 of 0.938 and RMSE of 0.038 N/mm², while ARIMA–HW closely followed with R^2 = 0.944 and RMSE = 0.032 N/mm². The superior performance of ARIMA–ANFIS is attributed to its sequential decomposition strategy, in which ARIMA captures the linear strength development trend associated with cement hydration, while ANFIS effectively models the nonlinear residual patterns arising from pozzolanic interactions and mixture-specific effects. The superiority of the hybrid approaches was further confirmed through Taylor diagram analysis, where ARIMA–ANFIS and ARIMA–HW predictions exhibited correlation coefficients approaching 0.99 with standard deviation ratios close to unity, indicating strong agreement between predicted and observed values. Overall, the proposed hybrid intelligence framework demonstrates strong potential as a reliable decision-support tool for optimizing sustainable concrete mixtures incorporating agro-industrial waste materials, enabling accurate compressive strength prediction while reducing the need for extensive experimental testing.

Competing Interests: The authors declare that they have no competing interests.

Data Availability Statement: The supported data associated with this researcher is available upon request from the corresponding author.

Acknowledgements: The authors gratefully acknowledge the Department of Civil Engineering, Kano University of Science and Technology, Wudil, for providing laboratory facilities and technical support throughout this investigation.

References

[1] P. J. M. Monteiro, S. A. Miller, and A. Horvath, “Towards sustainable concrete,” *Nat. Mater.*, vol. 16, no. 7, pp. 698–699, 2017.
[2] C. Meyer, “The greening of the concrete industry,” *Cem. Concr. Compos.*, vol. 31, no. 8, pp. 601–605, 2009.
[3] R. M. Andrew, “Global CO 2 emissions from cement production,” vol. 1, no. 10, pp. 195–217, 2018.
[4] E. Benhelal, E. Shamsaei, and M. I. Rashid, “Challenges against CO2 abatement strategies in cement industry: A review,” *J. Environ. Sci.*, vol. 104, pp. 84–101, 2021.
[5] M. S. Imbabi, C. Carrigan, and S. McKenna, “Trends and developments in green cement and concrete technology,” *Int. J. Sustain. Built Environ.*, vol. 1, no. 2, pp. 194–216, 2012.
[6] M. Schneider, “The cement industry on the way to a low-carbon future,” *Cem. Concr. Res.*, vol. 124, p. 105792, 2019.
[7] S. Chandra and L. Berntsson, *Lightweight aggregate concrete*. Elsevier, 2002.
[8] N. U. Kockal and T. Ozturan, “Durability of lightweight concretes with lightweight fly ash aggregates,” *Constr. Build. Mater.*, vol. 25, no. 3, pp. 1430–1438, 2011.
[9] F. Anwar *et al.*, “COMPRESSIVE STRENGTH OF LIGHTWEIGHT CONCRETE AND BENEFIT OF PARTIALLY REPLACING CEMENT BY ANIMAL BONE ASH (ABA),” *J. Emerg. Technol. Innov. Res.*, vol. 6, no. 6, pp. 554–560, 2019, [Online]. Available: www.jetir.org
[10] K. Jayathilakan, K. Sultana, K. Radhakrishna, and A. S. Bawa, “Utilization of byproducts and waste materials from meat, poultry and fish processing industries: a review,” *J. Food Sci. Technol.*, vol. 49, no. 3, pp. 278–293, 2012.
[11] F. Falade, E. Ikponmwosa, and C. Fapohunda, “Potential of Pulverized Bone as a Pozzolanic material.,” 2012.
[12] A. M. Neville, *Properties of concrete*, vol. 4. Longman London, 1995.
[13] D. Hernández-Cruz *et al.*, “Multiscale characterization of chemical-mechanical interactions between polymer fibers and cementitious matrix,” *Cem. Concr. Compos.*, vol. 48, pp. 9–18, Apr. 2014, doi: 10.1016/j.cemconcomp.2014.01.001.
[14] I.-C. Yeh, “Modeling of strength of high-performance concrete using artificial neural networks,” *Cem. Concr. Res.*, vol. 28, no. 12, pp. 1797–1808, 1998.
[15] P. Ziolkowski and M. Niedostatkiewicz, “Machine learning techniques in concrete mix design,” *Materials (Basel).*, vol. 12, no. 8, p. 1256, 2019.
[16] F.-J. Ulm and O. Coussy, “Modeling of thermochemomechanical couplings of concrete at early ages,” *J. Eng. Mech.*, vol. 121, no. 7, pp. 785–794, 1995.
[17] O. Bernard, F.-J. Ulm, and E. Lemarchand, “A multiscale micromechanics-hydration model for the early-age elastic properties of cement-based materials,” *Cem. Concr. Res.*, vol. 33, no. 9, pp. 1293–1309, 2003.
[18] D. S. Aliyu, C. T. Davie, and E. Masoero, “Influence of UV-treated polypropylene fibres on residual compressive strength of cement paste,” *Smart Sustain. Solut. Mater. Res. Forum LLC Mater. Res. Proc.*, vol. 48, pp. 359–367, 2025, doi: 10.21741/9781644903414-40.
[19] J.-S. Chou, C.-F. Tsai, A.-D. Pham, and Y.-H. Lu, “Machine learning in concrete strength simulations: Multi-nation data analytics,” *Constr. Build. Mater.*, vol. 73, pp. 771–780, 2014.
[20] W. Ben Chaabene, M. Flah, and M. L. Nehdi, “Machine learning prediction of mechanical properties of concrete: Critical review,” *Constr. Build. Mater.*, vol. 260, p. 119889, 2020.

[21] D. S. Aliyu, S. I. Malami, F. H. Anwar, M. M. Farouk, M. S. Labbo, and S. I. Abba, "Prediction of compressive strength of lightweight concrete made with partially replaced cement by animal bone ash using artificial neural network," in *2021 1st International Conference on Multidisciplinary Engineering and Applied Science, ICMEAS 2021*, Institute of Electrical and Electronics Engineers Inc., 2021. doi: 10.1109/ICMEAS52683.2021.9692317.

[22] H. Adeli, "Neural networks in civil engineering: 1989–2000," *Comput. Civ. Infrastruct. Eng.*, vol. 16, no. 2, pp. 126–142, 2001.

[23] H. Salehi and R. Burgueño, "Emerging artificial intelligence methods in structural engineering," *Eng. Struct.*, vol. 171, pp. 170–189, 2018.

[24] S. I. Abba *et al.*, "Emerging evolutionary algorithm integrated with kernel principal component analysis for modeling the performance of a water treatment plant," *J. Water Process Eng.*, vol. 33, Feb. 2020, doi: 10.1016/j.jwpe.2019.101081.

[25] I. B. Topçu and M. Saridemir, "Prediction of rubberized concrete properties using artificial neural network and fuzzy logic," *Constr. Build. Mater.*, vol. 22, no. 4, pp. 532–540, Apr. 2008, doi: 10.1016/j.conbuildmat.2006.11.007.

[26] M.-Y. Cheng and M.-T. Cao, "Accurately predicting building energy performance using evolutionary multivariate adaptive regression splines," *Appl. Soft Comput.*, vol. 22, pp. 178–188, 2014.

[27] J.-S. Chou, N.-T. Ngo, and A.-D. Pham, "Shear strength prediction in reinforced concrete deep beams using nature-inspired metaheuristic support vector regression," *J. Comput. Civ. Eng.*, vol. 30, no. 1, p. 4015002, 2016.

[28] A. A. Basma, S. A. Barakat, and S. Al-Oraimi, "Prediction of cement degree of hydration using artificial neural networks," *ACI Mater. J.*, vol. 96, no. 2, pp. 167–172, 1999.

[29] C. Bilim, C. D. Atiş, H. Tanyildizi, and O. Karahan, "Predicting the compressive strength of ground granulated blast furnace slag concrete using artificial neural network," *Adv. Eng. Softw.*, vol. 40, no. 5, pp. 334–340, 2009.

[30] H.-G. Ni and J.-Z. Wang, "Prediction of compressive strength of concrete by neural networks," *Cem. Concr. Res.*, vol. 30, no. 8, pp. 1245–1250, 2000.

[31] M. Saridemir, "Predicting the compressive strength of mortars containing metakaolin by artificial neural networks and fuzzy logic," *Adv. Eng. Softw.*, vol. 40, no. 9, pp. 920–927, 2009, doi: 10.1016/j.advengsoft.2008.12.008.

[32] M. W. Gardner and S. R. Dorling, "Artificial neural networks (the multilayer perceptron)—a review of applications in the atmospheric sciences," *Atmos. Environ.*, vol. 32, no. 14–15, pp. 2627–2636, 1998.

[33] Q. B. Pham *et al.*, "Potential of Hybrid Data-Intelligence Algorithms for Multi-Station Modelling of Rainfall," *Water Resour. Manag.*, vol. 33, no. 15, pp. 5067–5087, 2019, doi: 10.1007/s11269-019-02408-3.

[34] "Technical Summary of Vapnik (1998): Statistical Learning Theory," p. 1998, 1998.

[35] J. A. K. Suykens and J. Vandewalle, "Least squares support vector machine classifiers," *Neural Process. Lett.*, vol. 9, no. 3, pp. 293–300, 1999.

[36] K. Yan and C. Shi, "Prediction of elastic modulus of normal and high strength concrete by support vector machine," *Constr. Build. Mater.*, vol. 24, no. 8, pp. 1479–1485, 2010.

[37] M. A. Ghorbani, R. Khatibi, A. Goel, M. H. FazeliFard, and A. Azani, "Modeling river discharge time series using support vector machine and artificial neural networks," *Environ. Earth Sci.*, vol. 75, no. 8, p. 685, 2016.

[38] Daha S. Aliyu Haruna Ibrahim, M. M. Farouq, Hafizu H. Ali, "Performance of hybrid ANFIS and numerical simulation to predict the effect of steel fibre on compressive strength of concrete," *Techno-computing J.*, vol. 1, no. 1, pp. 27–41, Jan. 2025, Accessed: Apr. 13, 2025. [Online]. Available: https://doi.org/10.71170/tecoj.2025.1.1.27-41

[39] J. S. R. Jang, "ANFIS: Adaptive-Network-Based Fuzzy Inference System," *IEEE Trans. Syst. Man Cybern.*, vol. 23, no. 3, pp. 665–685, 1993, doi: 10.1109/21.256541.

[40] H. Tanyildizi, F. Özcan, C. D. Atis, O. Karahan, and E. Uncuog, "Advances in Engineering Software Comparison of artificial neural network and fuzzy logic models for prediction of long-term compressive strength of silica fume concrete," vol. 40, pp. 856–863, 2009, doi: 10.1016/j.advengsoft.2009.01.005.

[41] B. Vakhshouri and S. Nejadi, "Prediction of compressive strength of self-compacting concrete by ANFIS models," *Neurocomputing*, vol. 280, pp. 13–22, 2018.

[42] Z. Keshavarz and H. Torkian, "Application of ANN and ANFIS Models in Determining Compressive Strength of Concrete," *J. Soft Comput. Civ. Eng.*, vol. 2, no. 1, pp. 62–70, Jan. 2018, doi: 10.22115/SCCE.2018.51114.

[43] Z.-H. Duan, S.-C. Kou, and C.-S. Poon, "Prediction of compressive strength of recycled aggregate concrete using artificial neural networks," *Constr. Build. Mater.*, vol. 40, pp. 1200–1206, 2013.

[44] F. Giri and E.-W. Bai, *Block-oriented nonlinear system identification*, vol. 1. Springer, 2010.

[45] A. Bashir *et al.*, "Civil and Environmental Engineering for Resilient Enhancing durability and sustainability in fly ash-slag concrete using advanced metaheuristic algorithms and explainable ML for compressive strength prediction," *Smart Sustain. Solut. Mater. Res. Forum LLC Mater. Res. Proc.*, vol. 48, pp. 378–386, 2025, doi: 10.21741/9781644903414-42.

[46] A. Wills, T. B. Schön, L. Ljung, and B. Ninness, "Identification of hammerstein–wiener models," *Automatica*, vol. 49, no. 1, pp. 70–81, 2013.

[47] Y. Zhu, "Estimation of an N–L–N Hammerstein–Wiener model," *Automatica*, vol. 38, no. 9, pp. 1607–1614, 2002.

[48] M. S. Gaya *et al.*, "Estimation of turbidity in water treatment plant using hammerstein-wiener and neural network technique," *Indones. J. Electr. Eng. Comput. Sci.*, vol. 5, no. 3, pp. 666–672, 2017, doi: 10.11591/ijeecs.v5.i3.pp666-672.
[49] G. E. P. Box, G. M. Jenkins, G. C. Reinsel, and G. M. Ljung, *Time series analysis: forecasting and control*. John Wiley & Sons, 2015.
[50] M. F. M. Zain, M. N. Islam, and I. H. Basri, "An expert system for mix design of high performance concrete," *Adv. Eng. Softw.*, vol. 36, no. 5, pp. 325–337, 2005.
[51] F. J. Abdu, D. S. Aliyu, S. I. Malami, J. Usman, A. Bashir, and S. I. Abba, "Metaheuristic Optimization Algorithms for the Control and Management of Arsenic Concentration in the Eastern Province of Saudi Arabia," in *IEEE International Conference on Emerging and Sustainable Technologies for Power and ICT in a Developing Society, NIGERCON*, Institute of Electrical and Electronics Engineers Inc., 2024. doi: 10.1109/NIGERCON62786.2024.10927073.
[52] G. P. Zhang, "Time series forecasting using a hybrid ARIMA and neural network model," *Neurocomputing*, vol. 50, pp. 159–175, 2003.
[53] D. H. Wolpert and W. G. Macready, "No free lunch theorems for optimization," *IEEE Trans. Evol. Comput.*, vol. 1, no. 1, pp. 67–82, 2002.
[54] V. Nourani, Ö. Kisi, and M. Komasi, "Two hybrid artificial intelligence approaches for modeling rainfall–runoff process," *J. Hydrol.*, vol. 402, no. 1–2, pp. 41–59, 2011.
[55] M. Khashei and M. Bijari, "A novel hybridization of artificial neural networks and ARIMA models for time series forecasting," *Appl. Soft Comput.*, vol. 11, no. 2, pp. 2664–2675, 2011.
[56] V. Nourani and M. Sayyah Fard, "Sensitivity analysis of the artificial neural network outputs in simulation of the evaporation process at different climatologic regimes," *Adv. Eng. Softw.*, vol. 47, no. 1, pp. 127–146, 2012, doi: 10.1016/j.advengsoft.2011.12.014.
[57] J.-S. Chou and A.-D. Pham, "Enhanced artificial intelligence for ensemble approach to predicting high performance concrete compressive strength," *Constr. Build. Mater.*, vol. 49, pp. 554–563, 2013.
[58] BS EN 197-4:2004, "Cement — Part 4: Composition, specifications and conformity criteria for low early strength blastfurnace cements," 2004.
[59] BS EN 12620:2002, "Aggregates for concrete," 2008.
[60] B. Standard, "BS 3148: 1980. Methods of Test for Water for Making Concrete."
[61] B. Standard and T. Information, "British Standard Testing hardened concrete — Part 3: Compressive strength of test specimens," 2003.
[62] M. T. Hagan and M. B. Menhaj, "Training feedforward networks with the Marquardt algorithm," *IEEE Trans. Neural Networks*, vol. 5, no. 6, pp. 989–993, 1994.
[63] J. Vandewalle, "Least Squares Support Vector Machine Classifiers," pp. 293–300, 1999.
[64] V. Nourani, G. Elkiran, J. Abdullahi, and A. Tahsin, "Multi-region Modeling of Daily Global Solar Radiation with Artificial Intelligence Ensemble," *Nat. Resour. Res.*, vol. 28, no. 4, pp. 1217–1238, 2019, doi: 10.1007/s11053-018-09450-9.
[65] G. Cybenko, "Approximation by superpositions of a sigmoidal function," *Math. Control. signals Syst.*, vol. 2, no. 4, pp. 303–314, 1989.
[66] K. E. Taylor, "Summarizing multiple aspects of model performance in a single diagram," *J. Geophys. Res. Atmos.*, vol. 106, no. D7, pp. 7183–7192, 2001.
[67] D. Hernández-Cruz *et al.*, "Multiscale characterization of chemical–mechanical interactions between polymer fibers and cementitious matrix," *Cem. Concr. Compos.*, vol. 48, pp. 9–18, 2014.